Scc2 and Scc3 promote distinct modes of topological association between cohesin and DNA

James E Collier[1], Maurici B Roig[1], Stanislav Yatskevich[1], Naomi J Petela[1], Jean Metson[1], Menelaos Voulgaris[1], Byung-Gil Lee[2], Jan Löwe[2] and Kim A Nasmyth[1*]

[1] Department of Biochemistry, University of Oxford, Oxford, OX1 3QU, UK

[2] MRC Laboratory of Molecular Biology, Cambridge CB2 0QH, UK

* Corresponding author. Email: ashley.nasmyth@bioch.ox.ac.uk

SUMMARY

In addition to extruding long loops of DNA, cohesin topologically entraps within its SMC-kleisin ring (S-K) individual DNAs during G1 and sister DNAs during S-phase. All three activities require two related hook-shaped proteins called Scc2 and Scc3. Using a combination of cysteine pair substitutions and thiol-specific crosslinking we provide a rigorous demonstration of entrapment activity in vitro. We show that Scc2 alone promotes entrapment of DNAs in the E-S and E-K compartments between ATP-bound engaged heads and the SMC hinge and associated kleisin respectively. This process does not require ATP hydrolysis nor is it accompanied by entrapment within S-K rings, which is a slower process that requires addition of Scc3 and is stimulated by ATP hydrolysis. Our findings reveal that Scc2 and Scc3 have distinct roles in the process of topological entrapment and suggest that transient entrapment of DNAs in E-S/E-K compartments precedes S-K entrapment and may also be a feature of cohesin complexes active in loop extrusion.

INTRODUCTION

Protein complexes containing SMC and kleisin subunits organise the spatial arrangement, or topology, of DNAs in most if not all living organisms (Nasmyth, 2001; Yatskevich et al., 2019). Best characterised are the eukaryotic cohesin and condensin complexes that are thought to organise chromosomal DNAs during interphase and mitosis respectively by a process of loop extrusion (Golfier et al., 2020). Cohesin in addition mediates the connections between sister DNAs that hold sister chromatids together during mitosis until their disjunction at the onset of anaphase (Oliveira et al., 2010; Uhlmann et al., 1999). Many clues as to their molecular mechanisms have emerged from structural studies. All contain a

pair of rod-shaped SMC proteins with a dimerisation domain known as the hinge at one end separated by a 50nm long anti-parallel intra-molecular coiled coil from an ABC-like ATPase domain at the other (Haering et al., 2002). Their association creates V-shaped dimers whose apical ATPase head domains are interconnected by a kleisin subunit (Scc1) whose N-terminal domain forms a three helical bundle with the coiled coil emerging from Smc3's ATPase head (Gligoris et al., 2014), called its neck, and whose C-terminal winged helical domain binds to the base (or cap) of Smc1's ATPase head to complete the ring (Haering et al., 2004).

Hinge dimerisation facilitates numerous other contacts between Smc1 and Smc3. First, their coiled coils interact with each other extensively, all the way from the hinge to the joint, a small break in the coiled coil roughly 5nm above the heads, effectively zipping up the coiled coils (Bürmann et al., 2019; Chapard et al., 2019; Diebold-Durand et al., 2017; Soh et al., 2015). This process leads to the juxtaposition of the Smc1 and Smc3 heads, which are loosely associated under these conditions (Chapard et al., 2019; Diebold-Durand et al., 2017). Second, their coiled coils fold around an elbow, which results in an interaction between the hinge and a section of the coiled coils approximately 10nm from the heads (Bürmann et al., 2019). Last but not least, the γ-phosphate of ATP bound to one ATPase head binds a signature motif on the other, resulting under appropriate conditions in engagement of the heads and a sandwiching of two molecules of ATP between them, a process that is a precondition for subsequent ATP hydrolysis (Arumugam et al., 2003; Lammens et al., 2004; Marcos-Alcalde et al., 2017). Head engagement is thought to disrupt coiled coil interactions, at least in the vicinity of the heads, yet the full extent of this disruption is not known.

The ATPase activities of SMC-kleisin complexes as well as all their biological functions in vivo depend on additional proteins that are recruited through their association with kleisin subunits and act by binding DNA and interacting with various SMC protein domains. In cohesin, this class of proteins consists of large hook-shaped proteins composed of HEAT repeats, known as Heat repeat containing proteins Associated With Kleisins (HAWKs) (Wells et al., 2017). Cohesin has three such HAWKs known as Scc2, Scc3, and Pds5. Scc3 (Tóth et al., 1999) is thought to be permanently bound to the complex while association of Scc2 and Pds5, whose occupancy is mutually exclusive, are more dynamic (Petela et al., 2018). Scc2 is essential for cohesin’s ATPase activity (Petela et al., 2018), for its loading onto

chromosomes (Ciosk et al., 2000), for maintaining cohesin's chromosomal association during G1 (Srinivasan et al., 2019), and for cohesin's ability to extrude loops in vitro (Davidson et al., 2019; Kim et al., 2019). However, Scc2 is not required to maintain cohesion during G2 or even establish cohesion during S phase from complexes previously associated with unreplicated DNAs (Srinivasan et al., 2019). Pds5 also has multiple functions. By recruiting Wapl, it promotes cohesin's dissociation from chromosomes, a process blocked by acetylation of Smc3 during S phase (Beckouët et al., 2016; Chan et al., 2012, 2013). Pds5 also promotes acetylation during S phase and inhibits deacetylation during G2 and thereby protects sister chromatid cohesion which would otherwise be destroyed by Wapl-mediated release (Chan et al., 2013) .

Though the mechanism by which cohesin extrudes loops remains mysterious, there is a clear and simple hypothesis as to how cohesin holds sister DNAs together, namely by entrapping them both inside the S-K ring created through the binding of a kleisin subunit to the ATPase heads of an Smc1/Smc3 heterodimer (Gruber et al., 2003; Haering et al., 2002). This model explains the key observation that cleavage of cohesin's kleisin subunit by separase, or any other site-specific protease for that matter, is sufficient to trigger sister chromatid disjunction at anaphase (Oliveira et al., 2010; Uhlmann et al., 2000). To measure such entrapment in yeast, we have substituted residues within all three interfaces that make up S-K rings by pairs of cysteine residues that can be crosslinked by the thiol-specific reagent bismaleimidoethane (BMOE). Around 20% of cohesin complexes can be crosslinked simultaneously at all three interfaces in vivo (Gligoris et al., 2014) and in post-replicative cells this is accompanied by formation of SDS-resistant structures that hold together the sister DNAs of circular minichromosomes, called catenated dimers or CDs (Chapard et al., 2019; Gligoris et al., 2014; Srinivasan et al., 2018). Because the two DNAs associated with CDs are not otherwise intertwined (Haering et al., 2008), they must be held together by cohesin through a topological mechanism, either by co-entrapment within a chemically circularised S-K ring or conceivably in a three-way Borromean ring containing a pair of sister DNA rings and an SDS-resistant S-K ring. Importantly, the study of numerous mutants has revealed a perfect correlation between CD formation and cohesion establishment (Srinivasan et al., 2018), suggesting that these structures are actually responsible for sister chromatid cohesion or at the very least are produced by a highly related mechanism. Using cysteine pairs that cross-link juxtaposed or J heads (not engaged) (Chapard et al., 2019), it has been established that sister DNAs are at least some of the time

entrapped between juxtaposed heads and the kleisin associated with them, namely within a J-K subcompartment of the S-K ring (see Fig. 1A for overview on different compartments).

Loading of cohesin onto minichromosomes during G1 leads to a different topological interaction, namely catenation of individual circular DNAs by chemically circularised S-K rings, known as catenated monomers or CMs. Though loading of cohesin throughout the genome is normally accompanied by CM formation on minichromosomes, cohesin complexes containing a hinge with mutations within its lumen that neutralises its positive charge can load throughout the genome but cannot form either CMs or CDs (Srinivasan et al., 2018), implying that stable chromosomal association is not necessarily synonymous with entrapment of DNAs within S-K rings. That cohesin can associate with DNA in a functional manner without being topologically entrapped within S-K rings is supported by the finding that loop extrusion in vitro can be mediated by a version of human cohesin whose Smc1, Smc3, and kleisin subunits are expressed as a single polypeptide and whose hinge interface has been crosslinked by BMOE (Davidson et al., 2019). Importantly, neither of the above observations exclude the possibility that cohesin usually associates with chromosomal DNAs by entrapping a loop within its S-K ring, a type of association that has been termed pseudo-topological.

Previous reports claiming entrapment of DNA within cohesin rings in vitro used salt resistance and sensitivity to cleavage as their criteria (Murayama and Uhlmann, 2014, 2015). However, neither property demonstrates that DNAs are actually entrapped within S-K rings and either could stem from other types of entrapment, example within E-S compartments, or merely from simple physical association. Using site-specific crosslinking, we describe here bona fide topological entrapment of DNAs within S-K rings in vitro. Both Scc2 and Scc3 are essential for this process, as are their abilities to bind DNA. The process is dependent on ATP binding and stimulated by its hydrolysis, a feature largely absent from previous assays (Minamino et al., 2018). Remarkably, Scc2 alone promotes the rapid and simultaneous entrapment of DNAs within E-S and E-K compartments in a process that is not accompanied by entrapment within S-K rings. Because E-S/E-K entrapment is an order of magnitude more rapid than S-K entrapment, we suggest that creation of the former by Scc2 may be a precursor to the latter, a process contingent on the action of Scc3. Our results therefore reveal key insights into the biochemical activities of Scc2 and Scc3 and suggest that the first step towards S-K entrapment involves DNA passing between the ATPase heads

prior to their engagement.

RESULTS

SMC-kleisin rings entrap circular DNA in vitro

We expressed cohesin trimers consisting of Smc1, Smc3, and Scc1 in insect cells using the baculovirus expression system (Fig. S1A). Scc3 was expressed separately because co-expression with trimers resulted in substoichiometric yields. We also expressed a version of Scc2 lacking its N-terminal domain (Scc2C). Though this form no longer binds Scc4, it is fully capable of activating cohesin's ATPase activity (Petela et al., 2018), and for simplicity we will refer to this as simply Scc2 throughout the text. To measure entrapment of DNAs inside S-K rings (Fig. 1A i), we introduced cysteine pairs within all three ring interfaces (Smc1K639C-Smc3E570C, Smc1G22C-Scc1A547C, and Smc3S1043C-Scc1C56) that enables them to be crosslinked using BMOE. Individual interfaces were crosslinked with efficiencies varying from 30 to 70% and by comparing the migration of proteins following crosslinking cysteine pairs at single (2C), double (4C), and triple (6C) interfaces, we identified a covalently circular species only produced when all three interfaces were crosslinked (Fig. 1B).

To measure DNA entrapment within cohesin's S-K compartment in vitro, 6C SMC-kleisin trimers were mixed with circular supercoiled DNAs, Scc2, and Scc3, and incubated for 40 min at 24°C following addition of ATP. BMOE was then added and the mixture placed on ice for 6 min after which proteins were denatured by adding SDS to a final concentration of 1% and heating at 70°C for 20 min. The DNA was then fractionated by agarose gel electrophoresis and visualised by ethidium bromide staining (Fig. 1C & D). Addition of 6C trimers to Scc2/Scc3/DNA mixtures greatly reduced the amount of DNA co-migrating with supercoiled monomers and produced a ladder of retarded DNA species, most likely caused by successive entrapment by one, two, three etc S-K rings (Fig. 1D).

We propose that the ladder corresponds to multiple cohesin rings entrapping individual DNAs and not entrapment of multiple DNAs by individual cohesin rings for two reasons. First, the DNA retardation roughly corresponds to the molecular weight of the cohesin ring. Moreover, retardation caused by entrapment within E-S compartments (see below), which contain only Smc1 and Smc3, is less than that caused by entrapment within S-K or E-K compartments, which contain Scc1 as well as Smc1 and Smc3 (see Fig. 6D). Second,

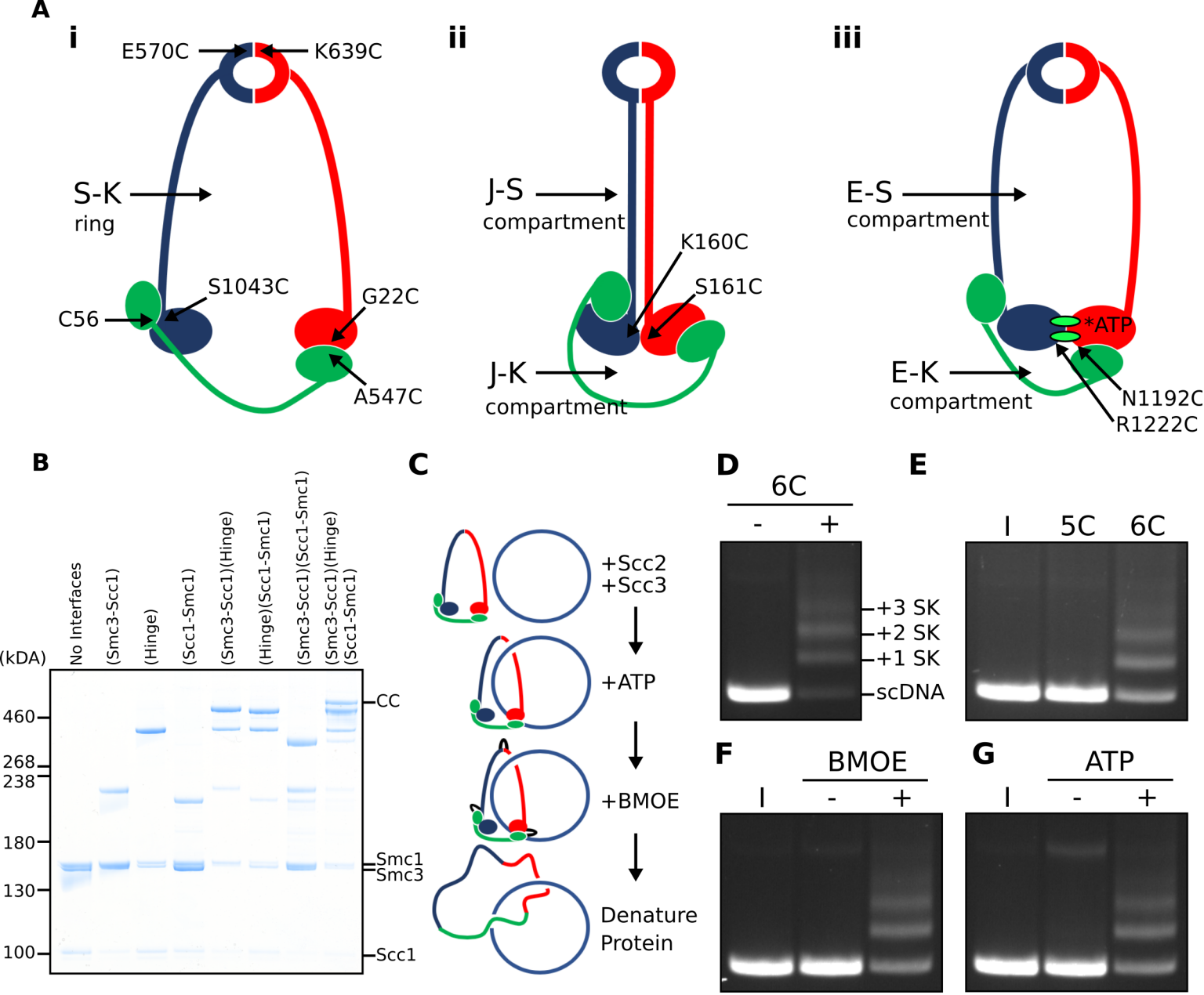
A
i
E570C
K639C
S-K
ring
S1043C
C56
G22C
A547C
ii
J-S
compartment
K160C
S161C
J-K
compartment
iii
E-S
compartment
*ATP
E-K
compartment
N1192C
R1222C
B
No Interfaces
(Smc3-Scc1)
(Hinge)
(Scc1-Smc1)
(Smc3-Scc1)(Hinge)
(Hinge)(Scc1-Smc1)
(Smc3-Scc1)(Scc1-Smc1)
(Smc3-Scc1)(Hinge)
(Scc1-Smc1)
(kDA)
460
268
238
180
130
100
CC
Smc1
Smc3
Scc1
C
+Scc2
+Scc3
+ATP
+BMOE
Denature
Protein
D
6C
-
+
+3 SK
+2 SK
+1 SK
scDNA
E
I
5C
6C
F
BMOE
I
-
+
G
ATP
I
-
+

Fig 1

Figure 1. SMC-kleisin (S-K) rings entrap circular DNA in vitro

(A) Schematic of the different compartments within cohesin and the position of cysteines. **(B)** BMOE crosslinking of S-K rings with cysteine pairs in the specified interfaces. CC = circular cohesin. (**C**) Schematic of the entrapment assay. (**D**) Entrapment of DNA in S-K rings in the presence of Scc2 and Scc3 and the presence or absence of 6C cohesin, or (**E**) the presence 5C cohesin lacking Scc1A547C, or 6C cohesin. (**F**) For DNA in the presence of Scc2, Scc3, and 6C cohesin and the presence or absence of BMOE, or (**G**) the presence or absence of ATP. Entrapment assays incubated for 40min (I = input DNA).

dimeric plasmid DNA, which is frequently present in plasmid preparations, although largely absent from these gels due to our purification protocol, runs roughly at the top of the gel with respect to our figures. Thus, if our ladders represented entrapment of multiple DNAs by individual cohesin rings, the DNA retardation should be much greater. Those DNAs retarded by entrapment within a single ring correspond to the CMs previously observed in vivo (Gligoris et al., 2014). Ladder formation required cysteine pairs at all three interfaces and was never observed when just a single cysteine (Fig. 1E) or BMOE (Fig. 1F) was omitted. Crucially, the ladders were strictly dependent on addition of ATP (Fig. 1G).

Entrapment of DNAs by S-K rings requires Scc3 and is stimulated by Scc2

To assess the roles of Scc2 and Scc3, we measured ladder formation at four successive 10-minute intervals in the presence and absence of the two proteins. Ladders indicative of entrapment increased with time (up to 40 min), suggesting that formation is a slow process, was greatly reduced by omission of Scc2 (Fig. 2A), and almost completely abolished by omission of Scc3 (Fig. 2B).

Entrapment of DNAs by S-K rings depends on ATP binding to Smc3 and on ATP hydrolysis

To address the role of cohesin's ATPase, we mutated Smc3's Walker A site (Smc3K38I) to abolish ATP binding to Smc3. This almost completely abolished entrapment (Fig. 2C). We did not test the effect of mutating the equivalent residue in Smc1 as this has previously been shown to abolish association of Smc1/3 heterodimers with Scc1 (Arumugam et al., 2003). We next tested the effect of mutating both Walker B sites to residues that permit ATP binding but not hydrolysis (Smc1E1158Q Smc3E1155Q) (Fig. S1B), which caused a more modest, albeit still significant, reduction (Fig. 2D). These data suggest that cohesin's ability to complete the ATP hydrolysis cycle stimulates entrapment but is not strictly necessary. To address whether Smc3's K112 and K113 are also important we analysed the effect of substituting them by glutamine (Smc3K112Q K113Q), mutations thought to mimic the acetylated state. This also reduced S-K entrapment (Fig. S1C), an effect that parallels its abrogation of cohesin loading in vivo (Hu et al., 2015).

DNA binding to Scc3 is required for its entrapment by S-K rings

During a search for cohesin domains that bind DNA, we discovered that Scc3's association with a fragment of Scc1 containing residues 269-451 greatly stimulates its association with

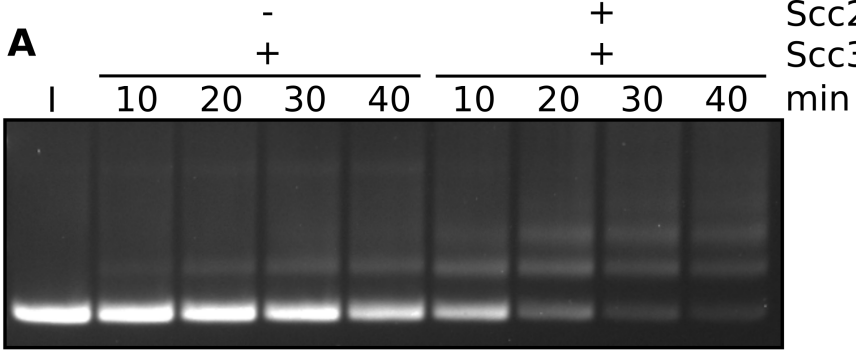
A
-
+
Scc2
+
+
Scc3
I
10
20
30
40
10
20
30
40
min

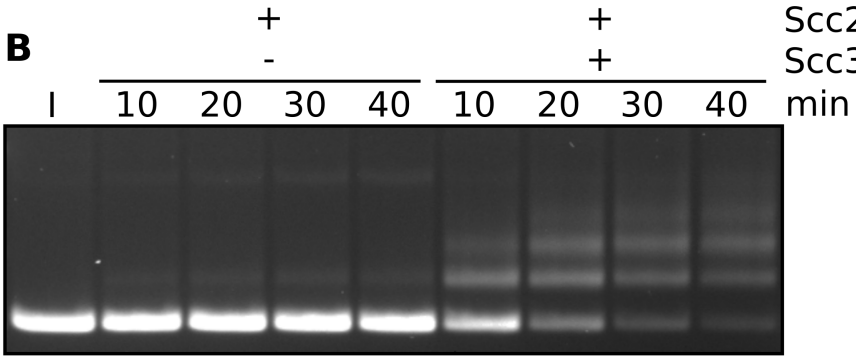
B
+
+
Scc2
-
+
Scc3
I
10
20
30
40
10
20
30
40
min

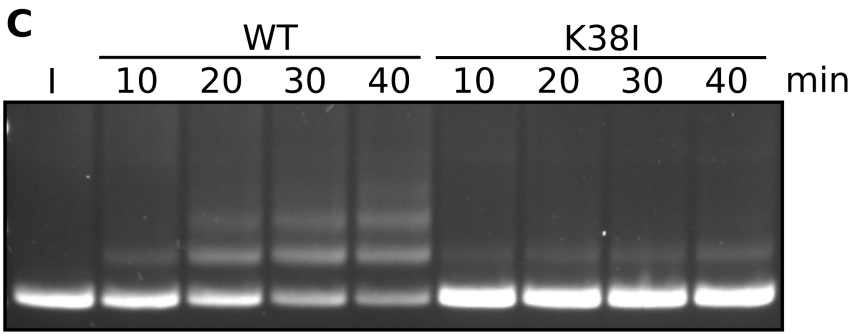
C
WT
K38I
I
10
20
30
40
10
20
30
40
min

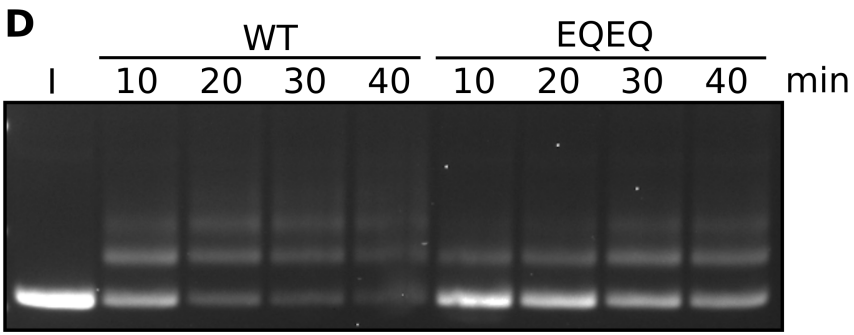
D
WT
EQEQ
I
10
20
30
40
10
20
30
40
min

Fig 2

Figure 2. Entrapment within S-K rings requires both Scc2 and Scc3, ATP binding to Smc3, and is stimulated by ATP hydrolysis

(**A**) Entrapment of DNA in S-K rings in the presence of Scc3, and the presence or absence of Scc2, or (**B**) the presence of Scc2, and the presence or absence of Scc3. (**C**) For DNA in S-K rings in the presence of Scc2 and Scc3, comparing WT cohesin to Smc3K38I (K38I), or (**D**) WT cohesin to Smc1E1158Q Smc3E1155Q (EQEQ). Entrapment assays incubated for 40min with time points taken every 10min (I = input DNA).

double stranded DNA, as measured using an electrophoretic mobility shift assay (EMSA) (Fig. S2A). Reasoning that Scc3/Scc1 complexes might bind DNA in a similar manner to that recently observed in a co-crystal of DNA bound to condensin's Ycg1 HAWK bound to its kleisin partner Brn1 (Kschonsak et al., 2017), we mutated two clusters of positively charged residues (Scc3K224E K225E R226E and Scc3 K423E K513E K520E) on opposite sides of the groove within Scc3 that is equivalent to Ycg1's DNA binding groove (Fig. 3A). Neither triple (3E) mutant eliminated DNA binding (Fig. S2B) nor caused lethality (Fig. S2E). Despite this, both reduced cohesin's association with all genomic sequences except point centromeres (*CEN*s) (Fig. S2C & D). In contrast, combining the two triple mutations (to create 6E) was lethal (Fig. S2E), abolished binding of Scc3 to DNA in the presence of Scc1 (Fig. 3B), and with the exception of *CEN*s eliminated cohesin's association with the genome (Fig. 3C & D).

Remarkably, cohesin containing Scc3-6E accumulated to exceptionally high levels at *CEN*s, (Fig. 3C & D) which are the loading sites for most peri-centric cohesin (50 kb intervals surrounding *CEN*s). This distribution resembles that of Scc2 in wild type cells and indeed, *scc3-6E* had little or no effect on Scc2's accumulation with *CEN*s (Fig. 3E). This implies that cohesin containing Scc3-6E forms complexes with Scc2 at *CEN*s but subsequently fails to form a stable association with chromatin or translocate into neighbouring sequences. Our ability to detect such complexes at *CEN*s but not at other loading sites along chromosome arms can be attributed to the fact that Scc2's partner Scc4 binds to the kinetochore protein Ctf19 and this association transiently tethers complexes at *CEN*s while they are attempting to load (Hinshaw et al., 2017). Though accumulation of cohesin bound by Scc2 at *CEN*s does not depend on Scc3's ability to bind DNA, it does still require Scc3 (Fig. S2F). Crucially, cohesin containing Scc3-6E failed to support entrapment of DNAs inside S-K rings in vitro (Fig. 3F). During the course of our work, a crystal structure of DNA bound to a Scc3/Scc1 complex confirmed that it does indeed bind DNA (Li et al., 2018 PDB 6H8Q) in a manner resembling that of Ycg1. Moreover, K224, K225 R226, K423, K513, and K520 are all predicted to contribute to the association. These data imply that Scc3's ability to bind DNA has an important role in cohesin's ability to load onto and translocate along chromosomal DNA in vivo, as well as entrap in S-K rings in vitro.

DNA binding to Scc2 facilitates entrapment by S-K rings

The *Schizosaccharomyces pombe* Scc2/4 complex has previously been shown to bind DNA

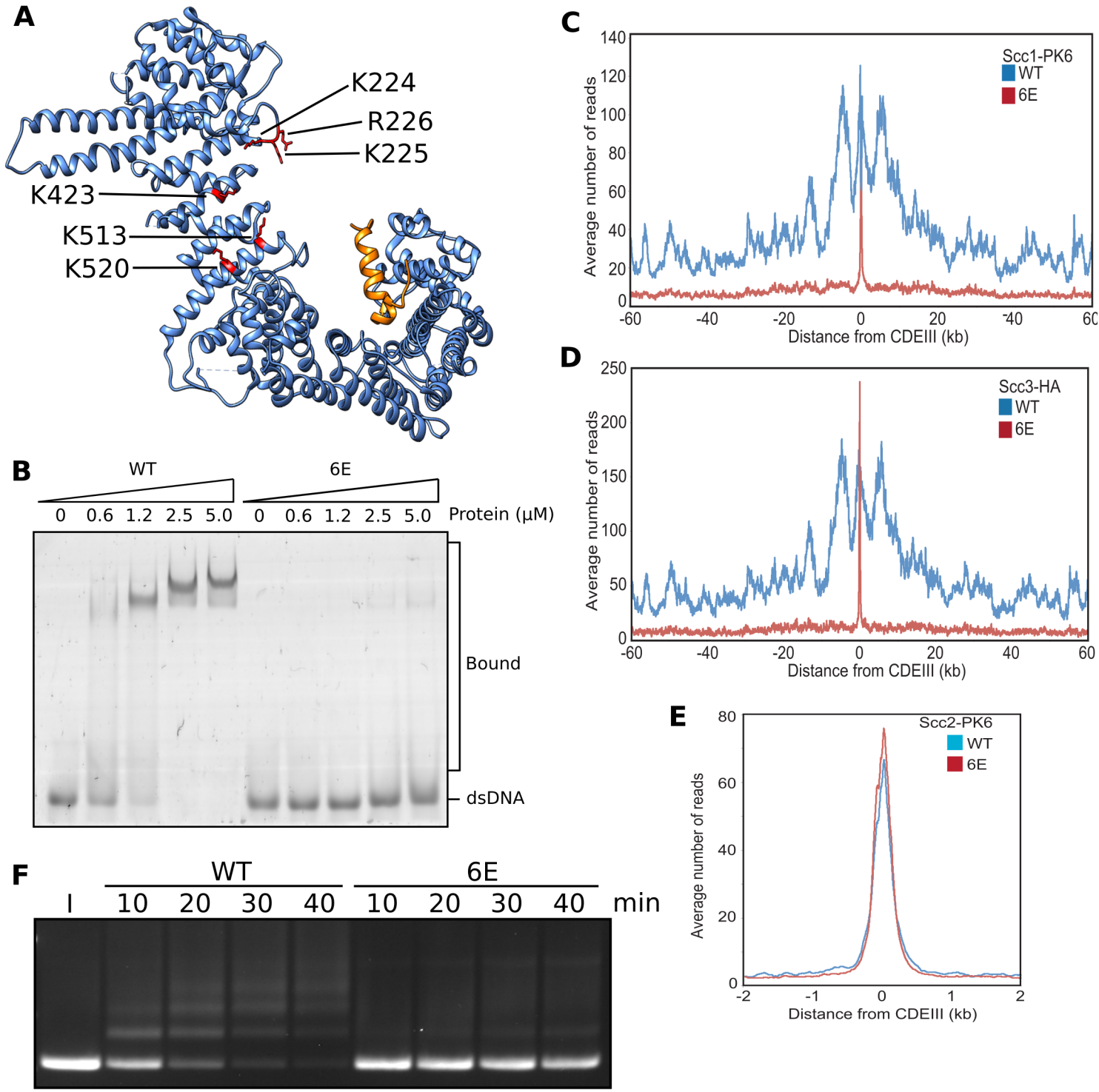
A
K224
R226
K225
K423
K513
K520
B
WT
6E
0 0.6 1.2 2.5 5.0 0 0.6 1.2 2.5 5.0
Protein (μM)
Bound
dsDNA
C
Scc1-PK6
WT
6E
Average number of reads
Distance from CDEIII (kb)
D
Scc3-HA
WT
6E
Average number of reads
Distance from CDEIII (kb)
E
Scc2-PK6
WT
6E
Average number of reads
Distance from CDEIII (kb)
F
WT
6E
I 10 20 30 40 10 20 30 40 min

Fig 3

Figure 3. DNA binding to Scc3 is required for its entrapment by S-K rings

(**A**) Structure of the *S. cerevisiae* Scc3 protein in complex with a fragment of Scc1 (PDB 6H8Q). Labelled are the six residues within the DNA binding groove of Scc3 that were mutated to glutamate (Scc3-6E). (**B**) EMSA comparing the ability of WT Scc3-Scc1$^{269-451}$ complexes to bind dsDNA against Scc3-6E-Scc1$^{269-451}$ complexes. (**C**) Average calibrated ChIP-seq profiles of Scc1-PK6 in the presence of WT Scc3 (KN27821) vs Scc3-6E (KN27804), or (**D**) Scc3-HA in the presence of WT Scc3 (KN27796) vs Scc3-6E (KN27802), or (**E**) Scc2-PK6 in the presence of WT Scc3 (KN28075) vs Scc3-6E (KN28287). All ChIP samples taken 60min after G1 release into auxin at 25°C. (**F**) Entrapment of DNA in S-K rings in the presence Scc2 and either WT Scc3 or Scc3-6E. Entrapment assay incubated for 40min with time points taken every 10min. (I = input DNA).

in vitro (Murayama and Uhlmann, 2014) but the physiological significance of this activity has never been investigated. EMSA revealed that *Saccharomyces cerevisiae* Scc2 also binds DNA (Fig. 4A), as do Scc2/4 complexes with slightly higher affinity (Fig. S3A). Unlike Scc3, whose DNA binding was greatly enhanced by Scc1, DNA binding by Scc2 was reduced by addition of a Scc1 fragment ($Scc1^{150-298}$) that contains sequences necessary for Scc2-dependent loading in vivo (Fig. 4A) (Petela et al., 2018) Interestingly, the inhibitory effect of $Scc1^{150-298}$ was not observed in the binding of DNA to full length Scc2/4 (Fig. S3A), suggesting that DNA binding sites also exist in Scc4, or in sequences N-terminal of the deletion in our Scc2C construct.

An alignment of the crystal structure of *Ashbya gossypii* Scc2 with that of Ycg1/barren bound to DNA revealed not only a remarkable similarity in the overall shape of their hook-shaped HEAT repeats but also a set of potential DNA binding residues on the surface of the shallow concave groove corresponding to Ycg1's DNA binding pocket (Petela et al., 2018) (Fig. 4B). Four of these are particularly conserved and correspond to S717, K721, K788, and H789 in *S. cerevisiae*. Both *scc2S717L K721E* and *scc2K788E H789E* double mutants are lethal and abolish loading of cohesin throughout most of the genome (Petela et al., 2018 and Fig. S3C). To test whether these residues participate in binding DNA, we used EMSAs to measure the effect on DNA binding of mutating the above residues to glutamate. Both Scc2S717E K721E and Scc2K788E H789E double mutants reduced binding (Fig. S3B) but caused only a modest reduction in S-K entrapment (data not shown). In contrast, the quadruple mutant Scc2S717E K721E K788E H789E (Scc2-4E) not only greatly reduced DNA binding (Fig. 4C) but also S-K entrapment (Fig. 4D). These results suggest that Scc2's ability to bind DNA has a crucial role in entrapping DNA within S-K rings in vitro, an activity also required for loading cohesin onto chromosomes in vivo (Petela et al., 2018 and Fig. S3C). They also demonstrate that the stimulation of DNA entrapment within S-K rings by Scc2 is not merely an adventitious property of Scc2 but an activity dependent on conserved surface residues that have unambiguous physiological functions.

DNA is never entrapped in J-S and only rarely in J-K compartments

Using the Smc1S161C-Smc3K160C cysteine pair, cohesin's ATPase heads can also be efficiently crosslinked in the J-state (Chapard et al., 2019). Moreover, this crosslinking can be combined with simultaneous crosslinking of N- and C-terminal kleisin domains to Smc3

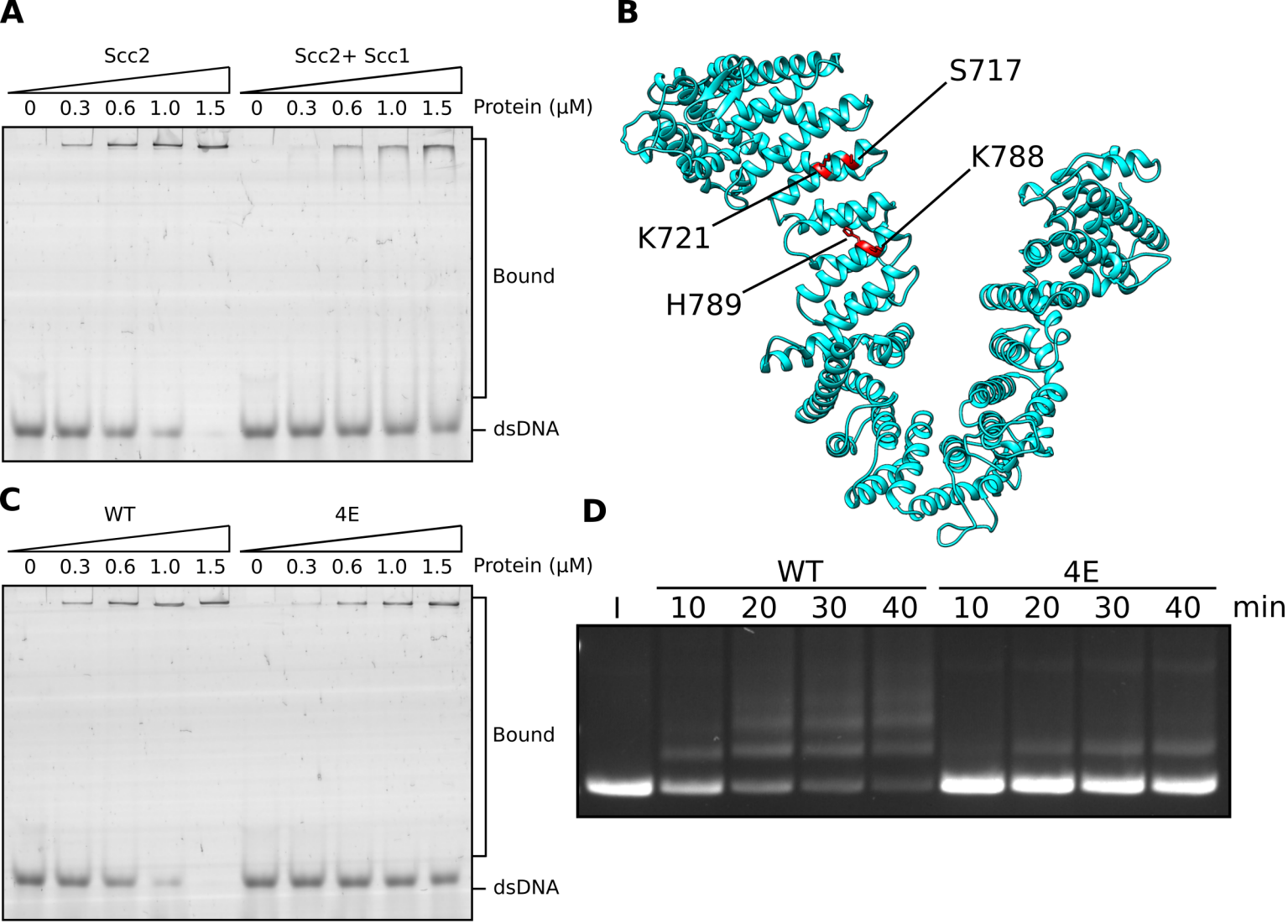
A
Scc2
Scc2+ Scc1
0 0.3 0.6 1.0 1.5 0 0.3 0.6 1.0 1.5
Protein (μM)
Bound
dsDNA
B
S717
K788
K721
H789
C
WT
4E
0 0.3 0.6 1.0 1.5 0 0.3 0.6 1.0 1.5
Protein (μM)
Bound
dsDNA
D
WT
4E
I 10 20 30 40 10 20 30 40 min

Fig 4

Figure 4. DNA binding to Scc2 facilitates entrapment by S-K rings

(**A**) EMSA comparing the ability of Scc2 to bind dsDNA against Scc2-Scc1$^{150-298}$ complexes, or (**B**) of WT Scc2 against Scc2-4E. (**C**) Model of *A. gossypii* Scc2$^{424-1476}$ (PDB 5ME3) with the *S. cerevisiae* Scc2 sequence mapped on top. Labelled are the four resides within the putative DNA binding surface that were mutated to glutamate (Scc2-4E). (**D**) Entrapment of DNA in S-K rings in the presence of Scc3 and either Scc2 or Scc2-4E. Entrapment assay incubated for 40min with time points taken every 10min. (I = input DNA).

and Smc1 ATPase heads respectively, to measure entrapment within J-K compartments (Fig. S4A), or with simultaneous crosslinking of the hinge (Fig. S4B), to measure entrapment of DNAs in J-S compartments (Fig. 1A ii). J crosslinking alone or in combination with hinge (J-S) or kleisin (J-K) was efficient even in the presence of ATP, DNA, Scc2, and Scc3 (Fig. S4C). In other words, both J-S and J-K circularisation occurred efficiently under conditions that promote efficient entrapment of DNAs inside S-K rings. DNAs were never entrapped within J-S compartments and only rarely by J-K ones (Fig. S4D). J-K entrapment was not only much lower than S-K entrapment but also independent of Scc2. The fact that J-K entrapment was comparable to S-K entrapment in the absence of Scc2 (compare Fig. 2A and S4D) suggests that the low-level entrapment of DNAs in S-K rings induced by Scc3 alone may in fact correspond to DNAs entrapped in J-K compartments. Though J-K circularisation by BMOE is modestly lower than that of S-K, this cannot account for its far lower DNA entrapment. We therefore suggest that most ATPase heads associated with DNA entrapped within S-K rings in vitro are not juxtaposed. They are either fully disengaged, in the engaged E-state, or in some other conformation.

Rapid DNA entrapment in E-S and E-K compartments

We used the same approach to measure entrapment in E-S or E-K compartments (Fig. 1A iii), in this case replacing J-specific cysteines by a pair specific for the engaged E-state (Smc1N1192C-Smc3R1222C). Unlike J crosslinking, which was readily detected in cohesin trimers, efficient E-state crosslinking was dependent on the presence of ATP (Fig. S5A). As with J-, E-state crosslinking can be combined with simultaneous crosslinking of N- and C-terminal kleisin domains to Smc3 and Smc1 ATPase heads respectively, to measure entrapment within E-K compartments (Fig. S5C), or with simultaneous crosslinking of the hinge (Fig. S5D), to measure entrapment of DNAs in E-S compartments. As previously reported (Chapard et al., 2019), Smc1/3 dimers crosslinked simultaneously at the hinge and E heads co-migrate with those crosslinked at the hinge alone, which hinders detection of E-S circularisation directly. Given that double crosslinking has been detected in vivo using differently tagged proteins (Chapard et al., 2019) and that DNAs are readily entrapped by Smc1/3 dimers containing hinge and E-specific cysteine pairs treated with BMOE, we can reason that efficient double crosslinking does indeed occur. DNAs were entrapped in an ATP-dependent fashion in both E-S and E-K compartments in the presence of Scc2 and Scc3 (Fig. 5A). Notably, both processes occurred much more rapidly than S-K entrapment, with significant amounts of DNA entrapped by multiple rings within 2 min (Fig. 5B). Because

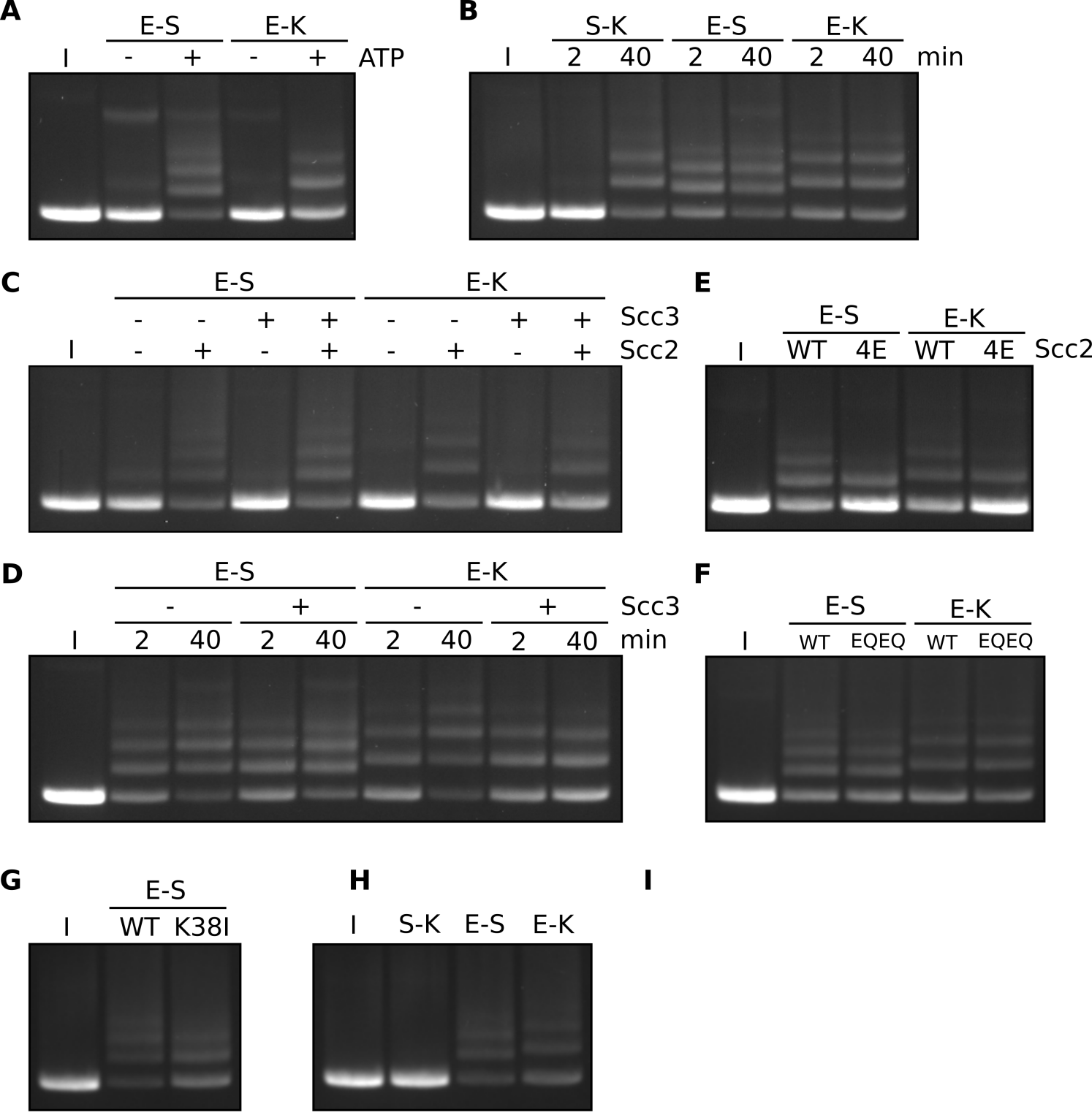
A
E-S
E-K
I
-
+
-
+
ATP
B
S-K
E-S
E-K
I
2
40
2
40
2
40
min
C
E-S
E-K
-
-
+
+
-
-
+
+
Scc3
I
-
+
-
+
-
+
-
+
Scc2
E
E-S
E-K
I
WT
4E
WT
4E
Scc2
D
E-S
E-K
-
+
-
+
Scc3
I
2
40
2
40
2
40
2
40
min
F
E-S
E-K
I
WT
EQEQ
WT
EQEQ
G
E-S
I
WT
K38I
H
I
S-K
E-S
E-K
I

Fig 5

Figure 5. Rapid DNA entrapment in E-S and E-K compartments

(**A**) Entrapment of DNA in E-S/E-K compartments in the presence of Scc2 and Scc3, and the presence or absence of ATP, incubated for 40min. (**B**) For DNA in S-K rings, or E-S/E-K compartments in the presence of Scc2 and Scc3, incubated for either 2 or 40min. (**C**) For DNA in E-S/E-K compartments in the presence of Scc2, Scc3, Scc2 and Scc3, or absence of both, incubated for 2min. (**D**) For DNA in E-S/E-K compartments in the presence of Scc2, and either the presence or absence of Scc3, incubated for either 2min or 40min. (**E**) For DNA in E-S/E-K compartments in the presence of either Scc2 or Scc2-4E, or (**F**) in the presence of Scc2, comparing entrapment by WT cohesin against Smc1E1158Q Smc3E1155Q (EQEQ), incubated for 2min. (**G**) For DNA in E-S compartments in the presence of Scc2 comparing entrapment by WT cohesin against Smc3K38I (K38I), or (**H**) for DNA in S-K rings, or E-S/E-K compartments in the presence of Scc2, incubated for 2min. (I = input DNA).

S-K entrapment occurs much more slowly, the efficient entrapment of DNAs inside E-S/E-K compartments within a few minutes is presumably not accompanied by S-K entrapment. Though it occurs efficiently in vitro, entrapment of circular DNAs by cohesin in E-S compartments has not so far been detected in vivo, although *Bacillus subtilis* SMC possessing Walker B mutations have been shown to have such an activity inside cells (Vazquez Nunez et al., 2019) .

Entrapment within the E-S and E-K compartments depends on Scc2 but not Scc3

In contrast to entrapment within S-K rings, which depends on Scc3, the rapid entrapment of DNA in the E-S/E-K compartments was Scc3 independent (Fig. 5C). However, it was highly dependent on Scc2 (Fig. 5C). Levels of E-S entrapment increased (albeit modestly) between 2 and 40 min in the presence of Scc2, as well as in the presence of Scc2 and Scc3 (Fig. 5D). However, while a similar result was seen for E-K entrapment in the presence of Scc2 alone, this increase was not observed in the presence of both Scc2 and Scc3 which instead showed no increase by the longer time point and possibly even a small reduction.

The rapid entrapment of DNAs within E-S/E-K compartments in the presence of Scc2 was reduced by Scc2-4E (Fig. 5E), suggesting that the reaction at least partly depends on Scc2's ability to bind DNA. Strikingly, both types of entrapment were unaffected by Smc1E1158Q *S*mc3E1155Q mutations (EQEQ), implying that neither form of entrapment requires ATP hydrolysis (Fig. 5F). In contrast to S-K entrapment in the presence of both Scc2 and Scc3 (Fig. 2C), E-S entrapment in the presence of Scc2 alone was only modestly reduced by Smc3K38I, implying that ATP bound merely to Smc1's ATPase head is sufficient (Fig. 5G). Indeed, Smc3K38I does not prevent E-state-specific crosslinking under these reaction conditions, namely in the presence of ATP, DNA, and Scc2 (Fig. S5E) and its modest reduction of E-S entrapment is in line with its effect on E-state crosslinking (Fig. 5G & S5E). Though it does not abolish head engagement, Smc3K38I clearly compromises the process. As long as ATP is present, neither DNA nor Scc2 are required for efficient E-state crosslinking of wild type complexes but both are important for Smc3K38I complexes (Fig. S5E). Smc3K38I presumably destabilises head engagement in a manner that can overcome by the presence of Scc2 and DNA. To explore whether Scc2 and DNA also promote head engagement of wild type complexes, we tested their effect when ATP's ability to promote head engagement is compromised by omission of Mg^{2+} (Fig. S5A & B). Under these

circumstances, addition of both Scc2 and DNA restored efficient head engagement and both factors were required for this effect (Fig. S5B). Our finding that Scc2 and DNA collaborate to promote ATP-dependent head engagement suggests that DNA binds to a groove on top of engaged heads as well as Scc2.

Scc2 causes DNAs to be entrapped in E-S and E-K compartments without entering S-K rings

Because Scc3 is crucial for S-K entrapment, the rapid entrapment of DNAs within E-S and E-K compartments in the presence of Scc2 alone should be unaccompanied by S-K entrapment. This is indeed the case. In contrast with E-S or E-K entrapment, which is very efficient, few if any DNAs are entrapped in S-K compartments by 2 min (Fig. 5H). Though paradoxical, this striking observation has a very simple explanation. The similarity in kinetics suggests that E-S and E-K entrapments are created simultaneously as part of the same reaction. In other words, a single type of DNA passage followed by head engagement gives rise to both types. We envisage two types of mechanism to explain how this occurs without S-K entrapment. According to the first and simplest, DNA moves “upwards” between disengaged ATPase heads, and is subsequently trapped in the E-S compartment following ATP-driven head engagement (Fig. 7A). An alternative is that a loop of DNA is inserted into an open S-K ring. If one of the loop’s segments were located above while the other below the ATPase domains, then subsequent head engagement would lead to simultaneous entrapment in both E-S and E-K compartments (Fig 7B). Neither type of DNA movement involves passage through a gate created by opening the S-K ring, hence explaining the lack of S-K entrapment.

Entrapment of DNA within E-S compartments disrupts coiled coil interactions proximal to the heads

To address whether the coiled coils are associated when Smc1/3 heads engage in vitro in the presence of Scc2, we combined the E-state-specific cysteine pair with one specific for the coiled coils (Smc1K201C-Smc3K198C), in close proximity to the joint. This revealed that double crosslinking can indeed occur in the presence of ATP (Fig. 6B). As expected, double crosslinking also occurred efficiently when the coiled coil pair was combined with one within the hinge interface (Smc1K639C-Smc3E570C). These cysteine pair combinations enabled us to measure entrapment within two sub-compartments within the E-S compartment (Fig.6A iii): one created by simultaneous crosslinking of the hinge and coiled coils (C-H

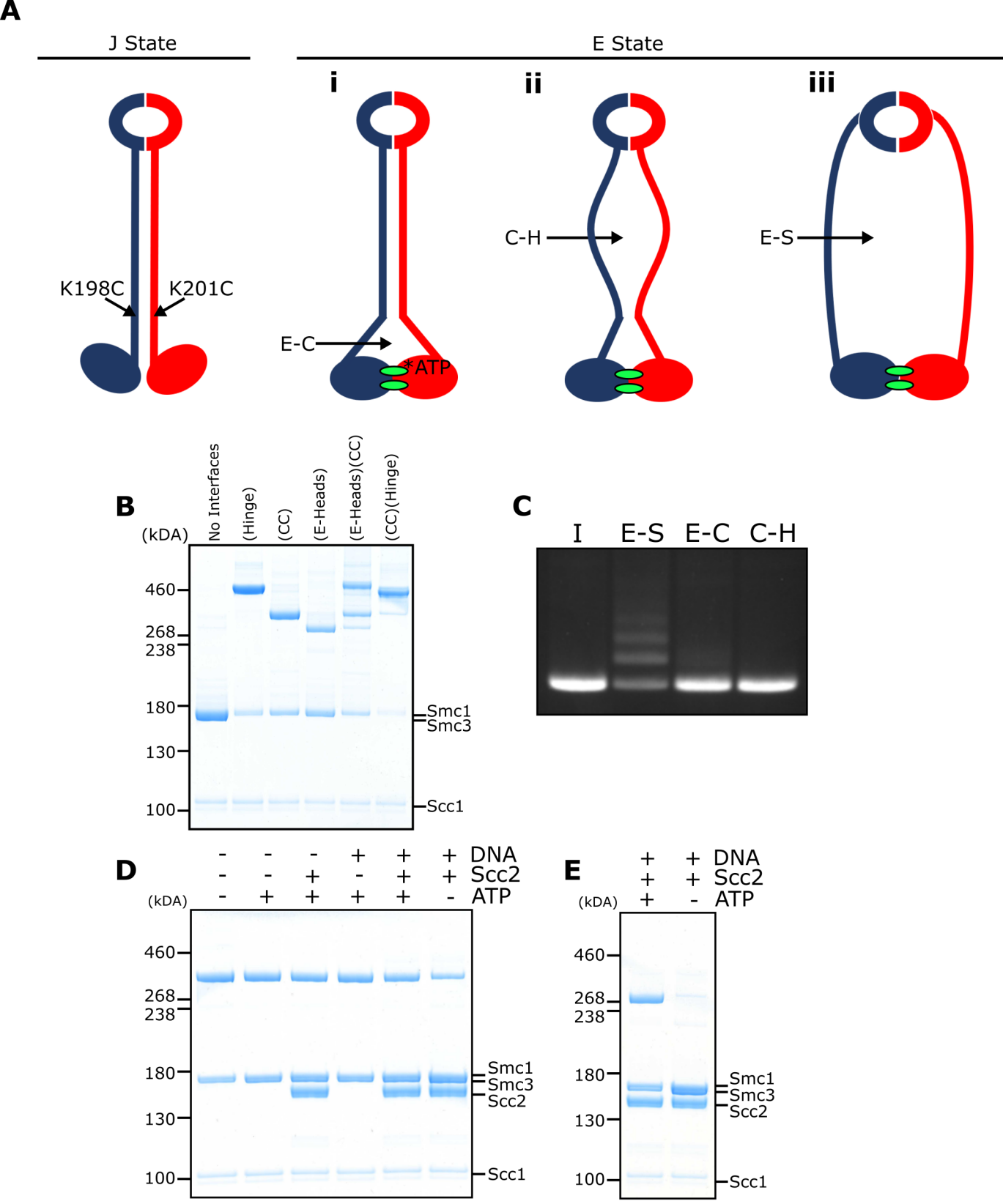
A
J State
E State
i
ii
iii
K198C
K201C
E-C
*ATP
C-H
E-S
B
(kDA)
No Interfaces
(Hinge)
(CC)
(E-Heads)
(E-Heads)(CC)
(CC)(Hinge)
460
268
238
180
130
100
Smc1
Smc3
Scc1
C
I
E-S
E-C
C-H
D
DNA
Scc2
ATP
Smc1
Smc3
Scc2
Scc1
E

Fig 6

Figure 6. Scc2 and DNA disrupt the J-state and E-S/E-K entrapment leads to dissociation of the coiled coil around the joint

(**A**) Schematic showing the location of the joint cysteine pair and how head engagement could lead to different degrees of coiled coil dissociation and subcompartment formation. (**B**) BMOE crosslinking of cohesin containing cysteine pairs in the specified interfaces in the presence of ATP. CC = coiled coils. (**C**) Entrapment of DNA in the E-S compartment, or either E-C or C-H subcompartments, in the presence of Scc2, incubated for 2min (I = input DNA). (**D**) BMOE crosslinking of cohesin with a cysteine pair specific for J head association, in the presence of ATP, DNA, or Scc2 in various combinations, or (**E**) containing a cysteine pair specific for E head association, in the presence of DNA, Scc2, and ATP, or DNA and Scc2.

compartment) (Fig. 6A ii) and a complementary one made by the simultaneous crosslinking of coiled coils and engaged heads (E-C compartment) (Fig. 6A i). If DNAs entrapped in E-S compartments are in versions whose coiled coils are associated, at least in the vicinity of their joint regions, then they must be entrapped either in the E-C or the H-C sub compartments. On the other hand, if the entrapment of DNAs within E-S compartments is accompanied by (or indeed causes), dissociation of the coiled coils in the vicinity of the Smc1K201C-Smc3K198C cysteine pair, then DNA should not be trapped in either of these sub-compartments.

Despite efficient crosslinking at both cysteine pairs (Fig. 6B), few if any DNAs were entrapped in the presence of Scc2 and ATP following BMOE treatment of cohesin trimers containing hinge and coiled coil cysteine pairs (Fig. 6C). Likewise, few if any DNAs were entrapped by cohesin trimers containing both E-state and coiled coil cysteine pairs. We deduce from this result that entrapment of DNAs within E-S compartments in the presence of Scc2 is accompanied by dissociation of their coiled coils in a manner that precludes crosslinking between Smc1K201C and Smc3K198C. Such dissociation would create space for DNA to bind to a positively charged groove created by head engagement, as observed in Mre11/Rad50 complexes (Liu et al., 2016), and more recently in both human and *S. pombe* cohesin (Fig. S6) (Higashi et al., 2020; Shi et al., 2020). We note that this conclusion based on cohesin's association with a large circular DNA is fully consistent with two cryo-EM structures of cohesin associated with Scc2/NIPBL and a small fragment of DNA, in which the two coiled coils diverge from each other at 70° as they emerge from their engaged heads (Higashi et al., 2020; Shi et al., 2020).

Scc2 and DNA disrupt the J-state in the absence of ATP

Passage of DNA between disengaged heads prior to ATP-driven head engagement would be essential for entrapment simultaneously in E-S and E-K compartments (see Discussion). There must therefore exist a mechanism by which the heads are moved sufficiently far apart to permit DNA passage. To investigate this, we tested the effect of ATP, Scc2, and DNA on crosslinking between the J-state cysteine pair. Conditions that promote efficient E-state crosslinking, namely addition of ATP, Scc2, and DNA, caused a modest 18.5% reduction in J-state crosslinking (Fig. 6D), confirming that the E-state is formed at the expense of J. As expected, other combinations of these three factors had less effect. Surprisingly, addition of

Scc2 and DNA in the absence of ATP had the greatest effect, causing a 53% reduction in J crosslinking, an effect that was highly reproducible. Such a marked reduction is presumably caused by the heads adopting a different conformation. Importantly, this does not correspond to the E-state as very little crosslinking takes place between Smc1N1192C and Smc3R1222C under these conditions (Fig. 6E). We therefore suggest that in the absence of ATP, both Scc2 and DNA reduce J-specific crosslinking by driving or indeed holding the ATPase heads apart, a process that could facilitate passage of DNA between them and thereby facilitate its entrapment in E-S compartments when heads engage in the presence of ATP.

DISCUSSION

Reproducing entrapment of DNA within cohesin SMC-kleisin rings in vitro

In vivo studies have shown that cohesin entraps circular minichromosomes within its S-K ring (Gligoris et al., 2014; Srinivasan et al., 2018). We demonstrate here that cohesin possesses such an activity also in vitro. Unlike previous assays that have merely measured the physical association between cohesin and DNA and investigated its resistance to salt or sensitivity to kleisin cleavage (Murayama and Uhlmann, 2014, 2015), our method measures topological association directly. By covalently circularising the cohesin ring and its component compartments we can make unambiguous deductions about the topology between DNA and cohesin. The entrapment of DNAs within S-K rings measured by this method depends on Scc2, Scc3, and ATP. Importantly, it is also stimulated by ATP hydrolysis, a feature that has been singularly lacking in previous assays but is of paramount importance for entrapment in vivo (Srinivasan et al., 2018). Four other key properties of the in vitro S-K entrapment activity reflect cohesin's behaviour in vivo, namely it depends on the ability of Scc2 and Scc3 to bind DNA, on the ability of ATP to bind Smc3 heads, and on Smc3's K112 and K113 residues, whose lack of acetylation is necessary for loading in yeast (Hu et al., 2015). We therefore suggest that the in vitro DNA S-K entrapment described here involves mechanisms similar or identical to those of cohesin operating within cells. If we assume that the efficiency of BMOE induced S-K circulation is around 20%, we estimate that many DNAs are entrapped by 15 or more cohesin rings in our assay after a 40 min incubation.

Potential mechanisms for Scc2-driven E-S/E-K entrapment

An obvious question concerns the state of the Smc1 and Smc3 ATPase heads when DNA

is entrapped. They could either be engaged in the presence of ATP, juxtaposed together in the absence of ATP (a state facilitated by extensive association of the Smc1 and Smc3 coiled coils), or fully disengaged. To address this, we used a Smc1-Smc3 cysteine pair specific for engaged heads, which revealed that DNAs are also entrapped efficiently between the hinge and engaged heads (the E-S compartment), between engaged heads and the kleisin subunit associated with them (the E-K compartment), but only rarely between juxtaposed heads and their associated kleisin (the J-K compartment). For obvious reasons, we were not able to address using cysteine-specific crosslinking whether DNAs are also entrapped within S-K rings with fully disengaged heads. However, given that cohesin's ability to hydrolyse ATP is important for S-K entrapment, it is likely that at least some S-K rings that have entrapped DNA in vitro are in this state. Our failure to observe efficient entrapment within J-K compartments was surprising given that this state has been documented in vivo (Chapard et al., 2019).

We were surprised to find that unlike entrapment within S-K rings, which requires Scc3, entrapment within E-S/E-K compartments was entirely Scc3 independent. In other words, entrapment within E-S/E-K compartments in the presence of Scc2 alone is not accompanied by entrapment within S-K rings. The similarity in kinetics suggests that entrapment within E-S and E-K compartments driven solely by Scc2 occurs simultaneously as part of the same reaction. The simplest explanation for this would be that DNA passes "up" between disengaged ATPase heads, and is then subsequently trapped in the E-S compartment following ATP-driven head engagement (Fig. 7A). The simultaneous entrapment within E-K compartments arises naturally from this, as the kleisin must be looped "upwards" to accommodate DNA entry in this manner. Crucially, this process would not require opening of the hinge or either SMC-kleisin interface, either of which would be necessary for entrapment within S-K rings.

Alternatively, simultaneous E-S/E-K entrapment could arise from a loop of DNA being inserted into an open S-K ring. If one segment of this loop were located above the heads, while the other located below them, head engagement would also lead to the simultaneous entrapment in E-S and E-K compartments (Fig. 7B). This scenario is not only more complex, but it must somehow explain how DNA is bent prior to insertion, a process which would carry a clear entropic penalty. Importantly, the states created by the two mechanisms are topologically isomeric. In other words, it is possible to transform the state described in Fig.

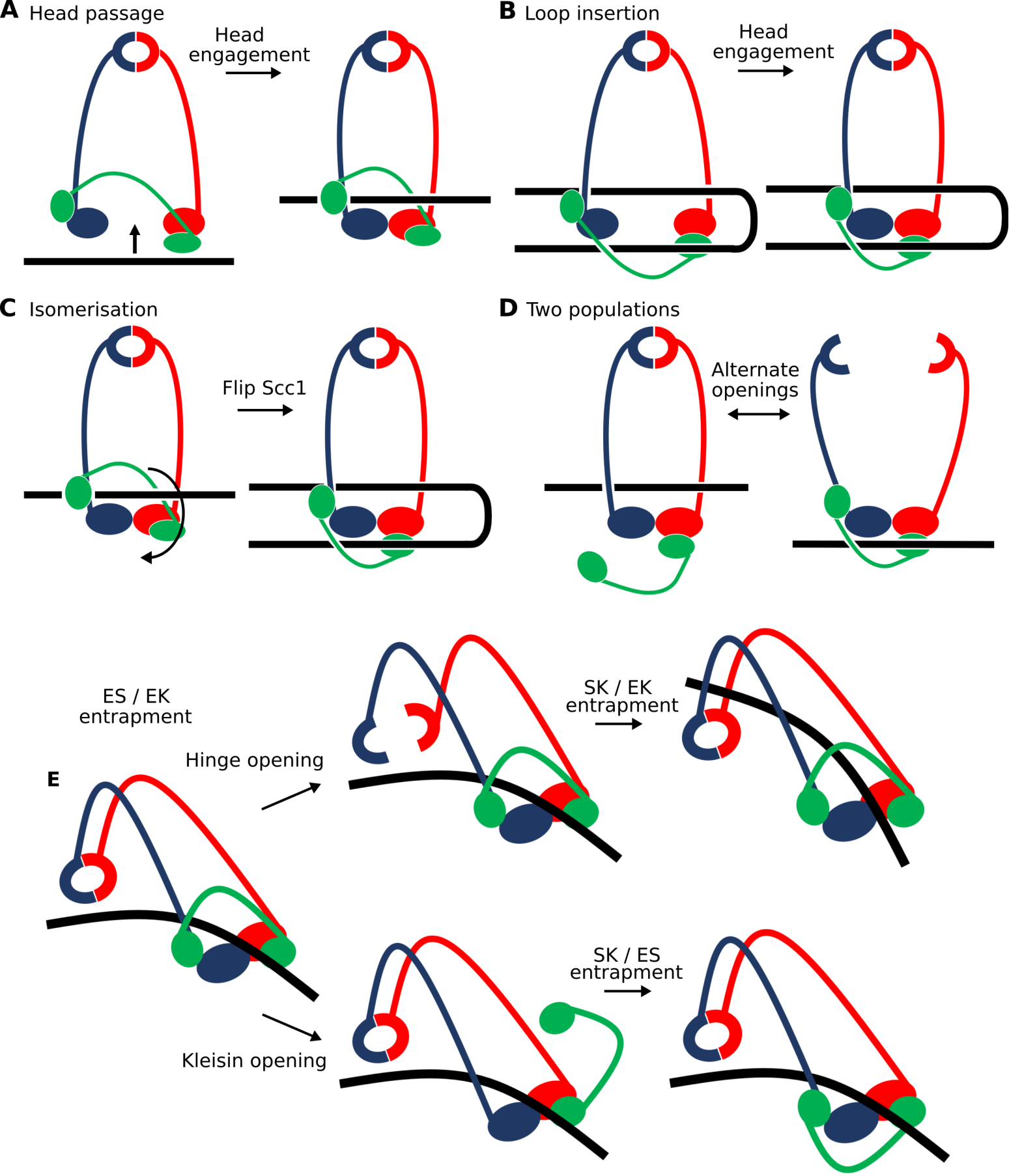
A Head passage
Head engagement
B Loop insertion
Head engagement
C Isomerisation
Flip Scc1
D Two populations
Alternate openings
E
ES / EK entrapment
Hinge opening
SK / EK entrapment
Kleisin opening
SK / ES entrapment

Fig 7

Figure 7. Potential mechanisms for Scc2-driven E-S and E-K entrapment and subsequent S-K ring entrapment

(**A**) ES/EK entrapment by DNA passing through open heads, or (**B**) through a DNA loop being inserted. (**C**) Topological isomerism between A and B. (D) ES/EK entrapment due to two distinct populations. (**E**) Models for converting E-S/E-K entrapment to S-K entrapment.

7A to that of Fig. 7B merely by moving Scc1's central domain "downwards" to below the heads and simultaneously bending the DNA through 180^0.

It is nevertheless important to point out that because our assays measuring E-S/E-K entrapment driven by Scc2 alone use complexes with different sets of cysteine pairs, they do not per se prove simultaneous entrapment of DNAs within both compartments. Thus, DNAs trapped in E-S/E-K compartments could in principle belong to separate populations (Fig. 7D). According to this scenario, and because E-S/E-K entrapment is not accompanied by S-K entrapment, DNAs entrapped solely within E-S compartments would have to be held by complexes whose kleisin subunit had dissociated from one or both ATPase heads while DNAs entrapped solely within E-K compartments would have to be trapped by complexes whose hinge had opened. It is unclear why head engagement in the presence of ATP, Scc2, and DNA should be associated with two such different events. A single mechanism that gives rise simultaneously to both types of entrapment without involving dissociation of any of the ring's interfaces is clearly a much simpler scenario. The notion that DNA can be engaged by cohesin rings in a manner that does not require opening of the hinge or either SMC-kleisin interface (Fig. 7A & B) is consistent with the recent observation that sealing all three interfaces does not adversely affect DNA loop extrusion by human cohesin complexes (Davidson et al., 2019) as well as the finding that the association between chromosomes and cohesin complexes with certain hinge mutations is not accompanied by S-K entrapment in vivo (Srinivasan et al., 2018).

If DNA does indeed pass through the ATPase domains, given that the heads are frequently associated, either in the E- or J-state, there must exist a mechanism to create an opening between them, if only transiently, in order for DNA to pass through. Our observation that Scc2 and DNA disrupts the J-state, albeit only in the absence of ATP, may be relevant in this regard (Fig 6D). This J-state disruption was not caused by adoption of the E-state (Fig. 6E), which requires ATP, and it must therefore involve transition to a state in which Smc1 and Smc3 ATPase heads adopt yet another conformation. This could be a state in which Scc2 and DNA together drive apart the ATPase head domains, thereby enabling DNA to pass between them. Subsequent ATP binding would then cause head engagement and E-state formation, trapping DNA inside both the E-S and E-K compartments. Interestingly, a conformation of this nature has recently been observed in condensin bound to Ysc4 (Lee et

al., 2020), where the latter bridges the Smc2 and Smc4 heads, holding them apart them by some distance. Although DNA was absent from this structure, the separation of the heads would be sufficient for DNA to pass between them.

We note that E-K entrapment would not be possible if Scc1's NTD were dissociated from Smc3's neck upon head engagement, as has been suggested by a cryo-EM structure of heads engaged in the absence of both DNA and Scc2 (Muir et al., 2020). The fact that E-K entrapment accompanies E-S entrapment during our Scc2-only reaction implies that Scc1's NTD does not in fact dissociate from Smc3's neck upon head engagement when DNA and Scc2 are present, as is also observed in recent human and *S. pombe* cryo-EM structures of cohesin heads in complex with DNA and NIPBL/Scc2 (Higashi et al., 2020; Shi et al., 2020). Because Scc2 is necessary to prevent cohesin's release from chromosomes during G1, and because release is accompanied by disengagement of Scc1's NTD from Smc3's neck (Srinivasan et al., 2019), we suggest that head engagement may indeed promote Scc1's dissociation from Smc3 but that this process is actively inhibited by Scc2. One of the functions of Pds5 and Wapl in mediating release during G1 when Smc3 is not acetylated may be to replace Scc2 and thereby abrogate this protection mechanism. In this regard, it is interesting that NIPBL's N-terminal domain contacts a short conserved loop just N-terminal to Scc1's NTD as well as the joint region within Smc3's coiled coil that is adjacent to Smc3's neck and Scc1's NTD. These two interactions could have a role in hindering Scc1's dissociation from Smc3 upon head engagement.

There are good reasons to believe that the circular DNAs entrapped in E-S/E-K compartments in our assays are bound to engaged heads and Scc2 in the same if not identical manner to that revealed by cryo-EM structures (Fig. S6) of DNA "gripped" by engaged heads and NIPBL/Scc2 (Higashi et al., 2020; Shi et al., 2020). As in these structures, E-S/E-K entrapment involves DNA binding to Scc2S717 K721 K788 and H789, it is unaffected by EQ mutations that abolish ATP hydrolysis, it involves Scc2 but not Scc3, and is accompanied by unzipping of Smc1 and Smc3 coiled coils in the neighbourhood of their joints. An important prediction of the cryo-EM structures is that by binding to engaged heads, DNA should facilitate head engagement. Likewise, by binding DNA and engaged heads, Scc2 should do likewise. Our finding that these factors do indeed cooperate in this manner and that this process is accompanied by the E-S/E-K DNA entrapment is a

compelling argument that E-S/E-K entrapment does indeed involve formation of the sort of structure observed by cryo-EM. One feature of E-S/E-K entrapment appears to differ from the human complex, namely opening of the north interface of the latter's hinge. Our E-S complexes, whether created in the presence or absence of Scc3, depend on BMOE-mediated cross-linking of a cysteine pair situated within the very same interface. It is important to point out that unlike the E-S/E-K entrapment described here, the cryo-EM structures did not reveal the topology of DNA's association with cohesin, because the coiled coils and large sections of the kleisins were not resolved and only a short oligonucleotide was bound.

Such a correspondence has another important implication, namely the demonstration that DNAs are simultaneously entrapped within E-S/E-K but not in S-K compartments is inconsistent with the proposal that DNAs pass through a transiently opened Scc1-Smc3 interface before they enter a "gripped" state created by head engagement (Higashi et al., 2020). Passage through a gate created by opening the Scc1-Smc3 interface before being "gripped" by engaged heads and Scc2 would be accompanied by E-K and S-K entrapment but not by E-S entrapment, which is contrary to what we observe. Either our E-S/E-K state does not in fact correspond to the "gripped" state observed in both human and fission yeast cryo-EM structures, which for the reasons outlined above seems unlikely, or the notion that its formation requires passage of DNA through the Scc1-Smc3 interface must be wrong.

Though Scc3 is present in the two aforementioned structures, there is no evidence that it is actually necessary for the binding of DNAs to engaged heads in the state described and we suggest that Scc2 alone is responsible. Ascertaining whether such structures can in fact be formed in the absence of Scc3, as our entrapment data suggest, is clearly an important priority. Moreover, it should be possible using the cysteine-specific crosslinking described in this paper to determine whether entrapment of circular DNAs within E-S/E-K compartments is accompanied by its entrapment within a channel created by Scc2's association with Smc3's coiled coil in the vicinity of its joint and with Smc3's head domain (Fig. S6). That Scc2 is required for S-K entrapment in the presence of Scc3, as well as E-S/E-K entrapment in its absence, suggest that entrapment driven by Scc2 and binding of DNA to engaged heads is necessary for subsequent S-K entrapment. However, this does not exclude the possibility that Scc2 has roles in S-K entrapment additional to formation of an E-S/E-K intermediate.

571

572 **Scc3 catalyses entry of DNA inside the SMC-kleisin ring**

573 Our finding that Scc3 is essential for S-K but not E-S/E-K entrapment reveals that Scc3 has
574 a unique role in promoting entry of DNA inside the SMC-kleisin ring. In principle, Scc3 could
575 catalyse DNA entry either via a gate created by transient hinge opening or through one
576 produced by transient dissociation of one or both SMC-kleisin interfaces (Fig. 7E). Crucially,
577 S-K entrapment in vivo is not abolished by fusing Scc1's NTD to Smc3 or by fusing its CTD
578 to Smc1, implying that DNA must enter either through the hinge or through dissociation of
579 either one of the two SMC-kleisin interfaces (possibly through simultaneous dissociation of
580 both) (Srinivasan et al., 2018). There is little or no direct evidence regarding which
581 mechanism is correct. SMC-kleisin dissociation has been strongly implicated in release and
582 is therefore also a plausible mechanism for entry (Beckouët et al., 2016). Nevertheless,
583 hinge opening is equally plausible, especially in the light of recent findings that folding of
584 cohesin's coiled coils around an elbow brings its hinge domain into close proximity to its
585 heads and that Scc3 interacts with a half opened hinge when DNA is bound to cohesin-
586 NIPBL complexes with engaged heads (Bürmann et al., 2019; Shi et al., 2020). Ascertaining
587 which mechanism is at play will require a method to measure the effect on S-K entrapment
588 of chemically linking interfaces together in a manner that is orthogonal to the BMOE-induced
589 crosslinking. For example, prior crosslinking of both SMC-kleisin interfaces would abolish
590 entrapment via a kleisin gate (Fig. 7E bottom pathway) but not via a hinge gate (Fig. 7E top
591 pathway).

592

593 This feature of Scc3's activity depends on it's ability to bind DNA in a manner similar to that
594 employed by Scc2 (this work, Li et al., 2018, Shi et al., 2020) and condensin's Ycg1 HAWK
595 (Kschonsak et al., 2017). Two sets of residues are implicated in DNA binding (K224 K225
596 R226 and K423 K513 K520). Mutation of one or other set does not abrogate DNA binding
597 or cause lethality but does reduce cohesin's association with chromosomes while mutation
598 of both sets (Scc3-6E) abolishes not only DNA binding and S-K entrapment in vitro but is
599 lethal and abolishes all loading throughout the genome in vivo. Though it abrogates
600 entrapment of DNA within S-K compartments (Fig. 3F), Scc3-6E has no effect on Scc2
601 driven E-S/E-K entrapment (data not shown). Thus, if S-K entrapment in vivo involved prior
602 formation of an E-S/E-K intermediate, which is consistent with the latter's more rapid kinetics
603 in vitro, then cohesin containing Scc3-6E should form this intermediate and accumulate in
604 this state, possibly at loading sites. Our observation that, despite failing to associate with

the vast majority of the genome, Scc3-6E cohesin accumulates at especially high levels at *CEN* sequences, which are highly efficient loading sites, suggests that this may indeed be the case. Unlike Scc3-6E, complete depletion of Scc3 abrogates cohesin's association at *CEN*s as well as along chromosomes arms, which implies that Scc3 has additional functions that do not involve or require its ability to bind DNA.

The notion that entrapment of DNA within S-K rings is preceded by its prior entrapment within E-K/E-S compartments, presumably bound to Scc2 and SMC heads in a manner observed in recent cryo-EM structures, raises the interesting possibility that DNA is eventually entrapped within the S-K ring, not by passing from outside to inside, but instead by being allowed to exit from either the E-S or the E-K compartment (without head disengagement) by opening transiently one of the S-K ring's three interfaces. Transient hinge opening would permit DNA's escape from the E-S compartment (Fig. 7E top pathway) while transient dissociation of one or another or indeed both kleisin-head interfaces would permit escape from the E-K compartment (Fig. 7E bottom pathway). In both cases, the subsequent closing of these exit gates would lead to entrapment of DNA within the S-K ring. According to these scenarios, exit via the hinge or via a SMC-kleisin interface without head disengagement would lead, at least initially, to the selective loss of E-S and E-K entrapment respectively. It is interesting in this regard that whereas E-K entrapment does not increase between 2 and 40 min when both Scc2 and Scc3 are present, E-S entrapment continues to increase in parallel with the rise in S-K entrapment. Whether this asymmetry is a hint that Scc3 promotes entrapment within S-K rings by opening an SMC-kleisin interface will require far more rigorous types of experiments. Though EQ mutants reduce S-K entrapment, they do not eliminate it, suggesting that DNA entry can in principle occur without head disengagement, as depicted in Fig. 7E.

The notion that a key function of Scc3 dependent on its ability to bind DNA is to facilitate entrapment of DNA within S-K rings has an important corollary. S-K entrapment is thought to be a crucial feature of sister chromatid cohesion. Hitherto, direct evidence for this mechanism has been confined to the observation of small circular minichromosomes entrapped within S-K rings in vivo. We show here that a function of Scc3, not shared by Scc2, is to facilitate entrapment within S-K rings. If this is also an essential function of Scc3 in vivo, it follows that S-K entrapment must also be an essential cohesin function and one that applies to proper chromosomes as well as small circular ones.

We have known for two decades that Scc2 and Scc3 have different roles in promoting cohesin's association with chromosomes (Ciosk et al., 2000; Tóth et al., 1999). The various topological assays described in this paper have finally revealed some of these. Scc2 promotes entrapment of DNA in E-S/E-K compartments by promoting its binding to engaged SMC ATPase heads, while Scc3 promotes entrapment inside S-K rings. Our findings are remarkably congruent with recent cryo-EM structures containing cohesin, DNA, and Scc2/NIPBL (Higashi et al., 2020; Shi et al., 2020). Crucially, they reveal the topology of DNA's association with cohesin, which cannot be discerned from these structures. Entrapment of DNAs within E-S compartments has not hitherto been detected in vivo, emphasizing the value of in vitro systems in revealing reactions that are otherwise difficult to detect. Future work will be required to address whether E-S/E-K entrapment also occurs inside cells, to elucidate the mechanism of S-K entrapment, and to reveal conditions that promote J-K entrapment, a form that has been detected in vivo but not yet efficiently in vitro.

ACKNOWLEDGEMENTS

Finally, we thank all members of the Nasmyth and Löwe groups for valuable discussions and many unseen contributions over the course of this work.

AUTHOR CONTRIBUTIONS

J.E.C. and K.A.N. conceived the study. J.E.C. conducted most the in vitro experiments and analysed the data, with contributions from M.B.R., S.Y., and M.V. In vivo experiments were carried out by M.B.R, N.J.P, and J.M. Cohesin purification protocol was developed by B.-G.L. and J.L. The manuscript was written by J.E.C. and K.A.N.

DECLARATION OF INTERESTS

The authors declare no competing interests.

MATERIALS AND METHODS

Recombinant yeast cohesin complex cloning

The *S. cerevisiae* genes *SMC1, SMC3, SCC3, SCC2, SCC1, and SCC4* were codon optimised for expression in *Spodoptera frugiperda* cells and synthesised using the Genscript Thermo Fisher Scientific service. These were then cloned into MultiBac vectors. Tag introduction and mutagenesis was achieved through Gibson assembly (New England

673 Biolabs) to generate *SMC1*-His, 2xStrepII-*SCC3*, *SCC1*-2xStrepII, *SCC2*-2xStrepII,
674 *SCC2*$^{133-1493}$-2xStrepII, and His-*SCC4*. *SMC3* *SMC1*-His, 2xStrepII-*SCC3, SCC2*-
675 2xStrepII, and *SCC2*$^{133-1493}$-2xStrepII were cloned into pACEbac1 vectors, and *SCC1*-
676 2xStrepII and His-*SCC4* cloned into pIDC vectors. *SMC1*-His and *SMC3* were then
677 combined into the same vector via cloning to create a pACEbac1 *SMC1*-His *SMC3*. Vectors
678 containing cohesin trimers were generated by combining pACEbac1 *SMC1*-His *SMC3* with
679 pIDC *SCC1*-2xStrepII by a Cre recombinase reaction (New England Bioloabs). The vector
680 for the Scc2/4 expression was also created by combining the pACEbac1 *SCC2*-2xStrepII
681 with pIDC His-*SCC4* using Cre recombinase.
682
683 **Virus generation and protein expression**
684 DNAs were first transformed into DH10Bac (ThermoFisher) cells and bacmids containing
685 the expression vector screened for by blue-white selection. DNA was then extracted and
686 2µg of bacmid DNA was infected into 2ml *S. frugiperda* Sf9 cells (ThermoFisher) at a cell
687 density of 1x10^{6} cells ml^{-1} using FuGENE HD reagent (Promega), grown in Sf900 II SFM
688 media (ThermoFisher). These were then incubated at 27°C for 5 days to create P1 virus. P2
689 virus was them amplified by infecting 50ml Sf9 cells at a density of 2x10^{6} cells ml^{-1} with
690 500µl P1 virus and incubating in the dark at 27°C for 3 days with shaking at 100rpm. P2
691 virus was then harvested by pelleting cells by centrifugation at 4000g and decanting into 5%
692 FBS (Sigma), and then stored in the dark at 4°C. Typically, proteins were then expressed by
693 adding 5ml P2 virus to 500ml Sf900 cells at a density of 2x10^{6} cells ml^{-1} and incubating in
694 the dark at 27°C for 2days with shaking at 100rpm. Cells were then harvested by
695 centrifugation at 1000g, washed with PBS, and then frozen in liquid N_2 and stored at -80°C.
696
697 **Cell lysis and protein purification**
698 Cells were thawed in Buffer A (50mM HEPES pH 7.5, 150mM NaCl, 1mM TCEP
699 (ThermoFisher), 5% glycerol) supplemented with 1 Complete Protease (EDTA-free) tablet
700 (Roche), 70µg RNAse A (Roche), and 100U ml^{-1} Supernuclease (SinoBiological) and then
701 lysed by sonication. Following sonication cell lysate was supplemented with 1mM PMSF
702 (Sigma). Proteins were then purified via a three strep purification protocol. First, proteins
703 were purified via affinity pulldown of their StrepII tags using a StrepTrap HP column (Fisher
704 Scientific) and eluted into Buffer A supplemented with 2.5mM desthiobiotin (Scc2 constructs
705 were eluted into 50mM Tris pH 8.0 rather than 50mM HEPES pH 7.5). Proteins were then

706 further purified by anion exchange chromatography using a 5ml HiTrap Q HP column (GE
707 Healthcare) across a gradient of 100mM to 1M NaCl (Scc2 constructs were eluted across a
708 gradient of 0mM to 1M NaCl). Finally, proteins were purified via size exclusion
709 chromatography using a Superose 6 increase 10/300 GL column (VWR) for cohesin trimers
710 and a HiLoad 16/60 Superdex column 200 (GE Healthcare) for Scc3 and the Scc2
711 constructs.
712
713 **Protein gel electrophoresis and western blotting**
714 Samples were mixed with 4xLDS sample buffer (ThermoFisher), loaded onto a 3-8% Tris-
715 acetate gel (ThermoFisher) and separated at 150V for 50min. Gels were then either stained
716 with Quick Coomassie stain (Generon) or transferred onto a 0.2µm nitrocellulose membrane
717 using a Trans-blot Turbo transfer pack (Bio-Rad). The antibodies used for western blotting
718 were anti-His (Sigma), anti-Strep HRP conjugated (iba). and anti-Smc3 (Bethyl
719 Laboratories). Primary antibodies were probed with anti-mouse HRP conjugated
720 (ThermoFisher).
721
722 **Purification of pUC19 plasmid DNA**
723 pUC19 plasmid was transformed into TOP10 (ThermoFisher) cells and grown overnight at
724 37°C. The next day a single colony was inoculated into 250ml SOB++ media and grown at
725 37°C overnight for 16 hours. DNA was then purified via MaxiPrep (Qiagen) using precooled
726 reagents and equipment and eluted into 50mM HEPES pH 7.5. DNA was then further
727 purified by $CsCl_2$ density gradient centrifugation in the presence of EtBr (ThermoFisher).
728 The DNA was then extracted, and the EtBr removed by washing several times with butanol
729 saturated with 50mM HEPES pH 7.5 and then the butanol phase discarded. The $CsCl_2$ was
730 then removed by dialysis against 2L 50mM HEPES pH 7.5 buffer over 24 hours at 4°C, with
731 two buffer changes. The DNA was then collected and stored at -20°C.
732
733 **Protein crosslinking assay**
734 For protein crosslinking assays, 10µl reactions were prepared containing 570nM protein
735 (buffered with 50mM HEPES pH 7.5, 50mM NaCl, 1mM $MgCl_2$, 1mM TCEP, 5% glycerol). If
736 added, ATP (Sigma) and supercoiled pUC19 were added to a concentration of 5mM and
737 120nM respectively. Reactions mixes were first incubated on ice for 5min before adding
738 BMOE (ThermoFisher) to a final concentration of 0.64mM (1µl BMOE added to 9µl protein
739 mix). Reactions were then incubated on ice for 6min. Samples were then denatured by

adding 4xLDS buffer and heating at 70°C for 10min before being separated in 3-8% Tris-acetate gels (ThermoFisher) run at 150V for 3 hours. Gels were then stained with Quick Coomassie stain (Generon).

DNA entrapment assay

For DNA entrapment assays, 13µl reactions were prepared containing 165nM protein and 9.3nM supercoiled pUC19 (buffered with 50mM HEPES pH 7.5, 20mM NaCl, 1mM $MgCl_2$, 5% glycerol). These were incubated on ice for 5min before reactions were initiated by addition ATP (Sigma) to a final concentration of 5mM (1µl ATP added to 12µl protein DNA mix). Typically, reactions were then incubated at 24°C for either 40min or 2min depending on the compartment being assessed. To these, 1.5µl BMOE (ThermoFisher) was added to a final concentration of 0.64mM and samples were incubated on ice for 6min. Samples were then denatured by addition of 1.5µl 10% SDS and heated at 70°C for 20min. DNA loading dye was then added and mixtures separated in a 0.8% agarose gel, run at 50V for 17hours at 4°C. The gel was stained with EtBr (ThermoFisher) and visualised by UV. Images shown are representative of 3 independent experiments.

ATPase assay

ATPase experiments were carried out as described in Petela et al., 2018.

Calibrated ChIP-sequencing

ChIP sequencing experiments were carried out as described in Petela et al., 2018.

Electromobility shift assay (EMSA)

A FAM-labelled 39 base pair HPLC purified DNA oligo (Invitrogen, GAATTCGGTGCGCATAATGTATATATTATGTTAAATAAGCTT) was annealed to a complementary DNA oligo to form dsDNA by heating to 95°C for 5min and then decreasing the temperature to 4°C in 0.1°C increments (buffered in 100mM potassium acetate, 50mM HEPES pH 7.5) to a final concentration of 45µM. The reactions were then prepared by adding 0.3µM FAM-dsDNA to increasing concentrations of protein (buffered in 50mM HEPES pH 7.5, 75mM NaCl, 1mM TCEP, 10% glycerol) in a final volume of 10µL. The reaction mix was then incubated on ice for 30min in the dark. These were then separated in 6% acrylamide gels prepared with 0.5% TAE (40mM Tris, 20mM acetic acid, 1mM EDTA)

run at 100V for 1 hour at 4°C in the dark. FAM-labelled DNA was visualised directly on a Fujifilm FLA7000 scanner with the LD473/Y[520] filter.

Cell viability of Scc3 mutants

Mutant *scc3* alleles (under its native promoter) were incorporated at the *leu2* locus in heterozygous *SCC3/Δscc3* cells. Diploids were sporulated and tetrads dissected onto YPD plates. The genotype of the resulting haploids was determined by replica plating. All mutations were confirmed by DNA sequencing.

REFERENCES

Arumugam, P., Gruber, S., Tanaka, K., Haering, C.H., Mechtler, K., and Nasmyth, K. (2003). ATP Hydrolysis Is Required for Cohesin's Association with Chromosomes. Curr. Biol. *13*, 1941–1953.

Beckouët, F., Srinivasan, M., Roig, M.B., Chan, K.L., Scheinost, J.C., Batty, P., Hu, B., Petela, N., Gligoris, T., Smith, A.C., et al. (2016). Releasing Activity Disengages Cohesin's Smc3/Scc1 Interface in a Process Blocked by Acetylation. Mol. Cell *61*, 563–574.

Bürmann, F., Lee, B.G., Than, T., Sinn, L., O'Reilly, F.J., Yatskevich, S., Rappsilber, J., Hu, B., Nasmyth, K., and Löwe, J. (2019). A folded conformation of MukBEF and cohesin. Nat. Struct. Mol. Biol. *26*, 227–236.

Chan, K.L., Roig, M.B., Hu, B., Beckouët, F., Metson, J., and Nasmyth, K. (2012). Cohesin's DNA exit gate is distinct from its entrance gate and is regulated by acetylation. Cell *150*, 961–974.

Chan, K.L., Gligoris, T., Upcher, W., Kato, Y., Shirahige, K., Nasmyth, K., and Beckouët, F. (2013). Pds5 promotes and protects cohesin acetylation. Proc. Natl. Acad. Sci. U. S. A. *110*, 13020–13025.

Chapard, C., Jones, R., van Oepen, T., Scheinost, J.C., and Nasmyth, K. (2019). Sister DNA Entrapment between Juxtaposed Smc Heads and Kleisin of the Cohesin Complex. Mol. Cell *75*, 224-237.e5.

Ciosk, R., Shirayama, M., Shevchenko, A., Tanaka, T., Toth, A., Shevchenko, A., and Nasmyth, K. (2000). Cohesin's Binding to Chromosomes Depends on a Separate Complex Consisting of Scc2 and Scc4 Proteins. Mol. Cell *5*, 243–254.

Davidson, I.F., Bauer, B., Goetz, D., Tang, W., Wutz, G., and Peters, J.-M. (2019). DNA loop extrusion by human cohesin. Science (80-.). *366*, 1338–1345.

Diebold-Durand, M.L., Lee, H., Ruiz Avila, L.B., Noh, H., Shin, H.C., Im, H., Bock, F.P.,

Bürmann, F., Durand, A., Basfeld, A., et al. (2017). Structure of Full-Length SMC and Rearrangements Required for Chromosome Organization. Mol. Cell *67*, 334-347.e5.

Gligoris, T.G., Scheinost, J.C., Bürmann, F., Petela, N., Chan, K.L., Uluocak, P., Beckouët, F., Gruber, S., Nasmyth, K., and Löwe, J. (2014). Closing the cohesin ring: Structure and function of its Smc3-kleisin interface. Science (80-.). *346*, 963–967.

Golfier, S., Quail, T., Kimura, H., and Brugués, J. (2020). Cohesin and condensin extrude DNA loops in a cell-cycle dependent manner. Elife *9*.

Gruber, S., Haering, C.H., and Nasmyth, K. (2003). Chromosomal cohesin forms a ring. Cell *112*, 765–777.

Haering, C.H., Löwe, J., Hochwagen, A., and Nasmyth, K. (2002). Molecular architecture of SMC proteins and the yeast cohesin complex. Mol. Cell *9*, 773–788.

Haering, C.H., Schoffnegger, D., Nishino, T., Helmhart, W., Nasmyth, K., and Löwe, J. (2004). Structure and stability of cohesin's Smc1-kleisin interaction. Mol. Cell *15*, 951–964.

Haering, C.H., Farcas, A.M., Arumugam, P., Metson, J., and Nasmyth, K. (2008). The cohesin ring concatenates sister DNA molecules. Nature *454*, 297–301.

Higashi, T.L., Eickhoff, P., Simoes, J.S., Locke, J., Flynn, H.R., Snijders, A.P., Papageorgiou, G., Reilly, O., Chen, Z.A., Reilly, F.J.O., et al. (2020). A Structure-Based Mechanism for DNA Entry into the Cohesin Ring. BioRxiv DOI 10.1101/2020.04.21.052944

Hinshaw, S.M., Makrantoni, V., Harrison, S.C., and Marston, A.L. (2017). The Kinetochore Receptor for the Cohesin Loading Complex. Cell *171*, 72-84.e13.

Hu, B., Petela, N., Kurze, A., Chan, K.L., Chapard, C., and Nasmyth, K. (2015). Biological chromodynamics: A general method for measuring protein occupancy across the genome by calibrating ChIP-seq. Nucleic Acids Res. *43*.

Kim, Y., Shi, Z., Zhang, H., Finkelstein, I.J., and Yu, H. (2019). Human cohesin compacts DNA by loop extrusion. Science (80-.). *366*, 1345–1349.

Kschonsak, M., Merkel, F., Bisht, S., Metz, J., Rybin, V., Hassler, M., and Haering, C.H. (2017). Structural Basis for a Safety-Belt Mechanism That Anchors Condensin to Chromosomes. Cell *171*, 588-600.e24.

Lammens, A., Schele, A., and Hopfner, K.-P. (2004). Structural Biochemistry of ATP-Driven Dimerization and DNA-Stimulated Activation of SMC ATPases. Curr. Biol. *14*, 1778–1782.

Lee, B., Merkel, F., Allegretti, M., Hassler, M., Cawood, C., Lecomte, L., Reilly, F.J.O., Sinn, L., Gutierrez-escribano, P., Bravo, S., et al. (2020). Cryo-EM structures of holo condensin reveal a subunit flip-flop mechanism. Nat. Struct. Mol. Biol. In Press

Li, Y., Muir, K.W., Bowler, M.W., Metz, J., Haering, C.H., and Panne, D. (2018). Structural

basis for scc3-dependent cohesin recruitment to chromatin. Elife *7*.

Liu, Y., Sung, S., Kim, Y., Li, F., Gwon, G., Jo, A., Kim, A., Kim, T., Song, O., Lee, S.E., et al. (2016). ATP -dependent DNA binding, unwinding, and resection by the Mre11/Rad50 complex . EMBO J. *35*, 743–758.

Marcos-Alcalde, Í., Mendieta-Moreno, J.I., Puisac, B., Gil-Rodríguez, M.C., Hernández-Marcos, M., Soler-Polo, Di., Ramos, F.J., Ortega, J., Pié, J., Mendieta, J., et al. (2017). Two-step ATP-driven opening of cohesin head. Sci. Rep. *7*, 1–14.

Minamino, M., Higashi, T.L., Bouchoux, C., and Uhlmann, F. (2018). Topological in vitro loading of the budding yeast cohesin ring onto DNA. Life Sci. Alliance *1*.

Muir, K.W., Li, Y., Weis, F., and Panne, D. (2020). The structure of the cohesin ATPase elucidates the mechanism of SMC–kleisin ring opening. Nat. Struct. Mol. Biol. *27*, 233–239.

Murayama, Y., and Uhlmann, F. (2014). Biochemical reconstitution of topological DNA binding by the cohesin ring. Nature *505*, 367–371.

Murayama, Y., and Uhlmann, F. (2015). DNA Entry into and Exit out of the Cohesin Ring by an Interlocking Gate Mechanism. Cell *163*, 1628–1640.

Nasmyth, K. (2001). Disseminating the Genome: Joining, Resolving, and Separating Sister Chromatids During Mitosis and Meiosis. Annu. Rev. Genet. *35*, 673–745.

Oliveira, R.A., Hamilton, R.S., Pauli, A., Davis, I., and Nasmyth, K. (2010). Cohesin cleavage and Cdk inhibition trigger formation of daughter nuclei. Nat. Cell Biol. *12*, 185–192.

Petela, N.J., Gligoris, T.G., Metson, J., Lee, B.G., Voulgaris, M., Hu, B., Kikuchi, S., Chapard, C., Chen, W., Rajendra, E., et al. (2018). Scc2 Is a Potent Activator of Cohesin's ATPase that Promotes Loading by Binding Scc1 without Pds5. Mol. Cell *70*, 1134-1148.e7.

Shi, Z., Gao, H., Bai, X., and Yu, H. (2020). Cryo-EM structure of the human cohesin-NIPBL-DNA complex. Science (80-.). eabb0981.

Soh, Y.M., Bürmann, F., Shin, H.C., Oda, T., Jin, K.S., Toseland, C.P., Kim, C., Lee, H., Kim, S.J., Kong, M.S., et al. (2015). Molecular basis for SMC rod formation and its dissolution upon DNA binding. Mol. Cell *57*, 290–303.

Srinivasan, M., Scheinost, J.C., Petela, N.J., Gligoris, T.G., Wissler, M., Ogushi, S., Collier, J.E., Voulgaris, M., Kurze, A., Chan, K.L., et al. (2018). The Cohesin Ring Uses Its Hinge to Organize DNA Using Non-topological as well as Topological Mechanisms. Cell *173*, 1508-1519.e18.

Srinivasan, M., Petela, N.J., Scheinost, J.C., Collier, J., Voulgaris, M., Roig, M.B., Beckouët, F., Hu, B., and Nasmyth, K.A. (2019). Scc2 counteracts a wapl-independent mechanism that releases cohesin from chromosomes during G1. Elife *8*, 1–34.

Tóth, A., Ciosk, R., Uhlmann, F., Galova, M., Schleiffer, A., and Nasmyth, K. (1999). Yeast cohesin complex requires a conserved protein, Eco1p(Ctf7), to establish cohesion between sister chromatids during DNA replication. Genes Dev. *13*, 320–333.

Uhlmann, F., Lottspelch, F., and Nasmyth, K. (1999). Sister-chromatid separation at anaphase onset is promoted by cleavage of the cohesin subunit Scc1. Nature *400*, 37–42.

Uhlmann, F., Wernic, D., Poupart, M.-A., Koonin, E. V, and Nasmyth, K. (2000). Cleavage of Cohesin by the CD Clan Protease Separin Triggers Anaphase in Yeast. Cell *103*, 375–386.

Yatskevich, S., Rhodes, J., and Nasmyth, K. (2019). Organization of Chromosomal DNA by SMC Complexes. Annu. Rev. Genet. *53*, 445–482.

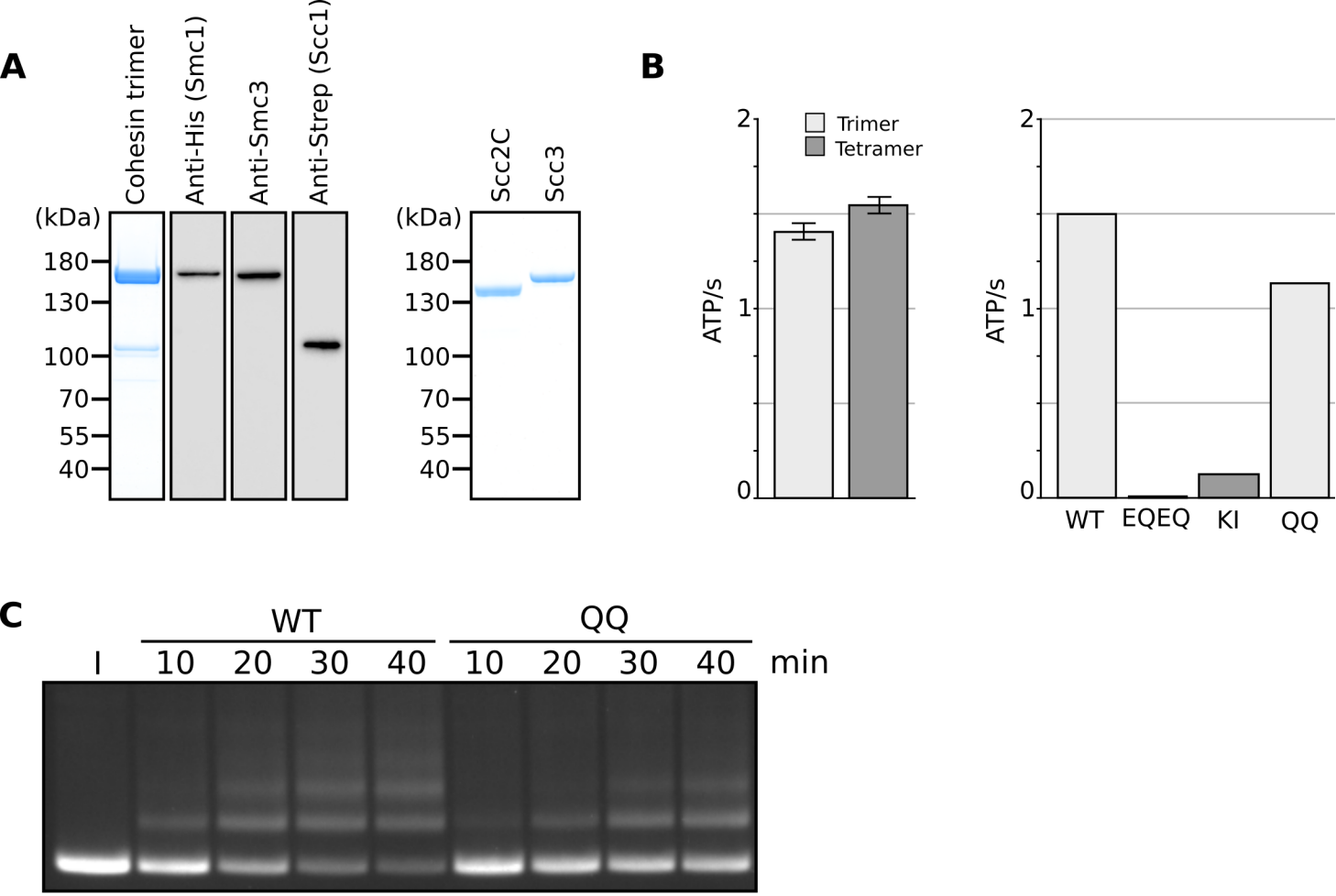
A
Cohesin trimer
Anti-His (Smc1)
Anti-Smc3
Anti-Strep (Scc1)
(kDa)
180
130
100
70
55
40
Scc2C
Scc3
B
Trimer
Tetramer
ATP/s
2
1
0
WT
EQEQ
KI
QQ
C
WT
QQ
I
10
20
30
40
min

Fig S1

Figure S1. Related to Figures 1 and 2

(**A**) Left hand panel - Coomassie strain of cohesin trimers. Individual subunits were then probed for by western blotting. Right hand panel – Coomassie stain of Scc2C and Scc3. (**B**) Left hand panel - ATPase activity for purified cohesin trimers incubated with DNA, Scc2, and ATP in the presence of Scc3 (tetramer) or absence (trimer). Right hand panel – ATPase activity for either WT cohesin tetramer, Smc1E1158Q Smc3E1155Q (EQEQ), Smc3K38I (KI) or Smc3K112Q K113Q (QQ). (**C**) Entrapment of DNA in S-K rings in the presence of Scc2 and Scc3 comparing WT cohesin to Smc3K112Q K113Q (QQ).

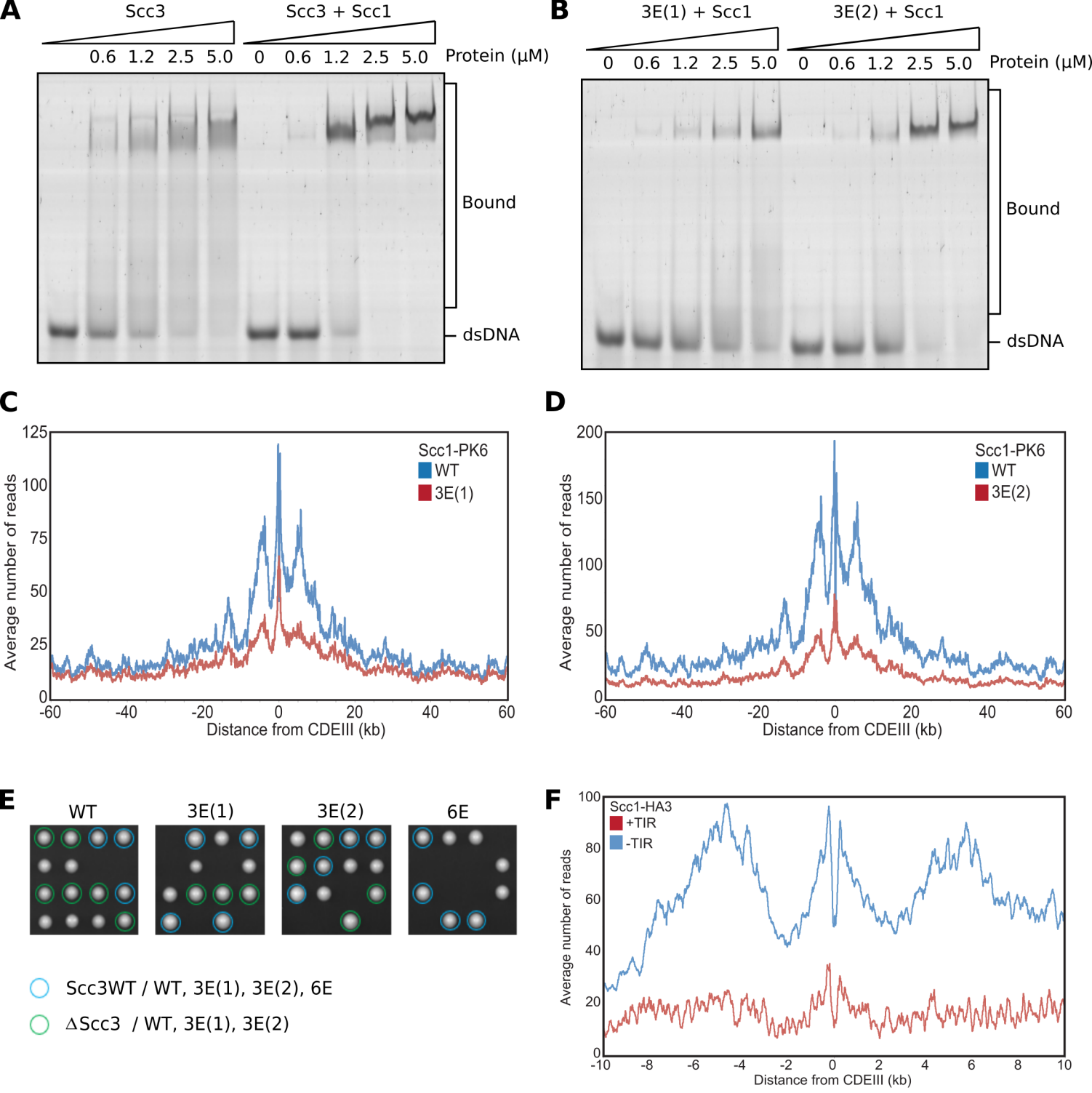
A
Scc3
Scc3 + Scc1
0.6 1.2 2.5 5.0
0 0.6 1.2 2.5 5.0
Protein (μM)
Bound
dsDNA
B
3E(1) + Scc1
3E(2) + Scc1
0 0.6 1.2 2.5 5.0
0 0.6 1.2 2.5 5.0
Protein (μM)
Bound
dsDNA
C
Scc1-PK6
WT
3E(1)
Average number of reads
Distance from CDEIII (kb)
D
Scc1-PK6
WT
3E(2)
Average number of reads
Distance from CDEIII (kb)
E
WT
3E(1)
3E(2)
6E
Scc3WT / WT, 3E(1), 3E(2), 6E
ΔScc3 / WT, 3E(1), 3E(2)
F
Scc1-HA3
+TIR
-TIR
Average number of reads
Distance from CDEIII (kb)

Fig S2

Figure S2. Related to Figure 3

(**A**) EMSA comparing the ability of Scc3 to bind dsDNA against Scc3-Scc1$^{269-451}$ complexes, or (**B**) of Scc3-3E(1)-Scc1$^{269-451}$ (Scc3K224E K225E R226E) against Scc3-3E(2)-Scc1$^{269-451}$ (Scc3K423E K513E K520E) complexes. (**C**) Average calibrated ChIP-seq profiles of Scc1-PK6 in the presence of WT Scc3 (KN27542) vs Scc3-3E(1) (KN27547), or (**D**) WT Scc3 (KN27542) vs Scc3-3E(2) (KN27697), taken from cycling cells at 25°C. (**E**) Vertical tetrad dissection of diploid cells expressing one copy of WT Scc3 from the endogenous locus and one copy of either WT Scc3 (KN21273), Scc3-3E(1) (KN27539), Scc3-3E(2) (KN27696), or Scc3-6E (KN27763) from an ectopic locus. WT Scc3, Scc3-3E(1), Scc3-3E(2) are able to support viability but Scc3-6E is not. Further marker selection, protein expression and genotype sequencing confirmed that Scc3-6E causes lethality. (**F**) Average calibrated ChIP-seq profiles of Scc1-HA3 either expressing TIR (KN20783) or not (KN20785), taken 60min after G1 release into auxin at 25°C.

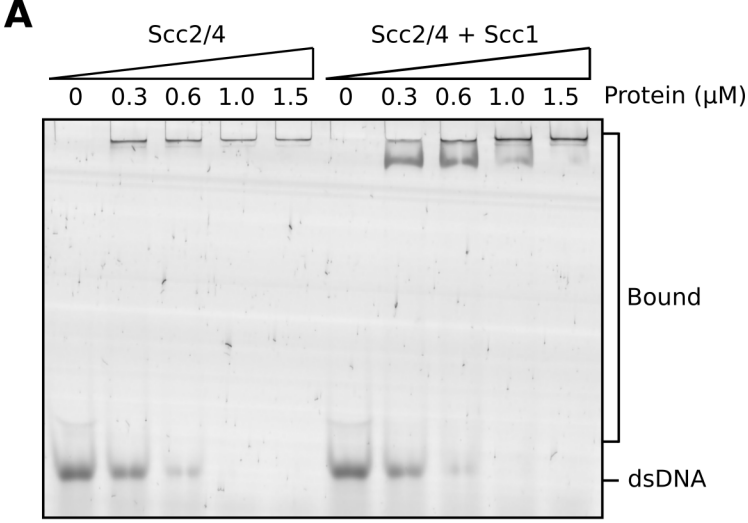
A
Scc2/4
Scc2/4 + Scc1
0 0.3 0.6 1.0 1.5 0 0.3 0.6 1.0 1.5
Protein (μM)
Bound
dsDNA

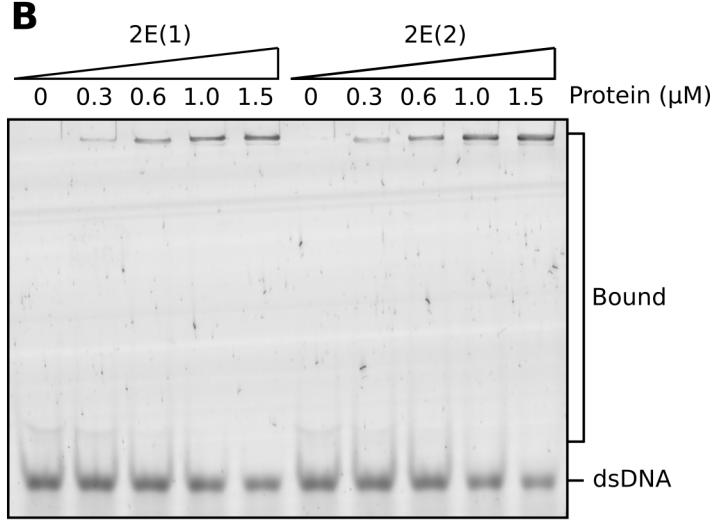
B
2E(1)
2E(2)
0 0.3 0.6 1.0 1.5 0 0.3 0.6 1.0 1.5
Protein (μM)
Bound
dsDNA

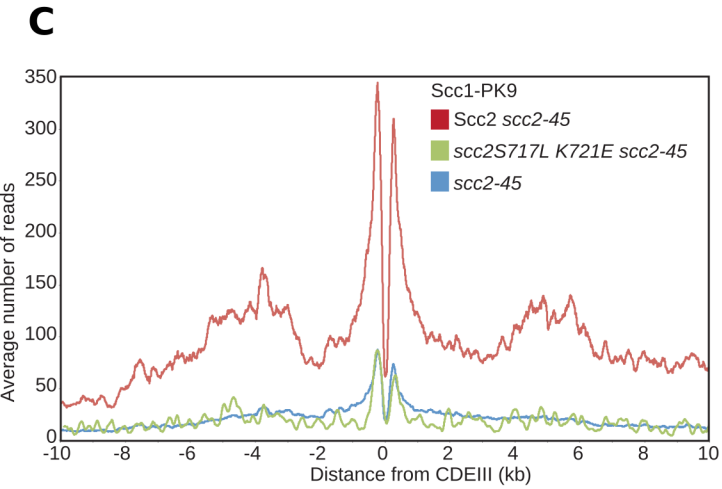
C
Scc1-PK9
Scc2 scc2-45
scc2S717L K721E scc2-45
scc2-45
Average number of reads
350
300
250
200
150
100
50
0
-10 -8 -6 -4 -2 0 2 4 6 8 10
Distance from CDEIII (kb)

Fig S3

Figure S3. Related to Figure 4

(**A**) EMSA comparing the ability of full length Scc2/4 complexes to bind dsDNA against Scc2/4-Scc1$^{150-298}$, or (**B**) of Scc2-2E(1) (Scc2S717E K721E) against Scc2-2E(2) (Scc2K788E H789E). (**C**) Average calibrated ChIP-seq profiles of Scc1-PK6 in the presence of *Scc2 scc2-45* (KN24185), *scc2-45* (KN22390), or *scc2S717L K721E scc2-45* (KN27010). Cells were arrested in G1 at 25°C before release into medium containing nocodazole at 37°C. Samples were taken 75min after release. *scc2-45* is a temperature sensitive allele.

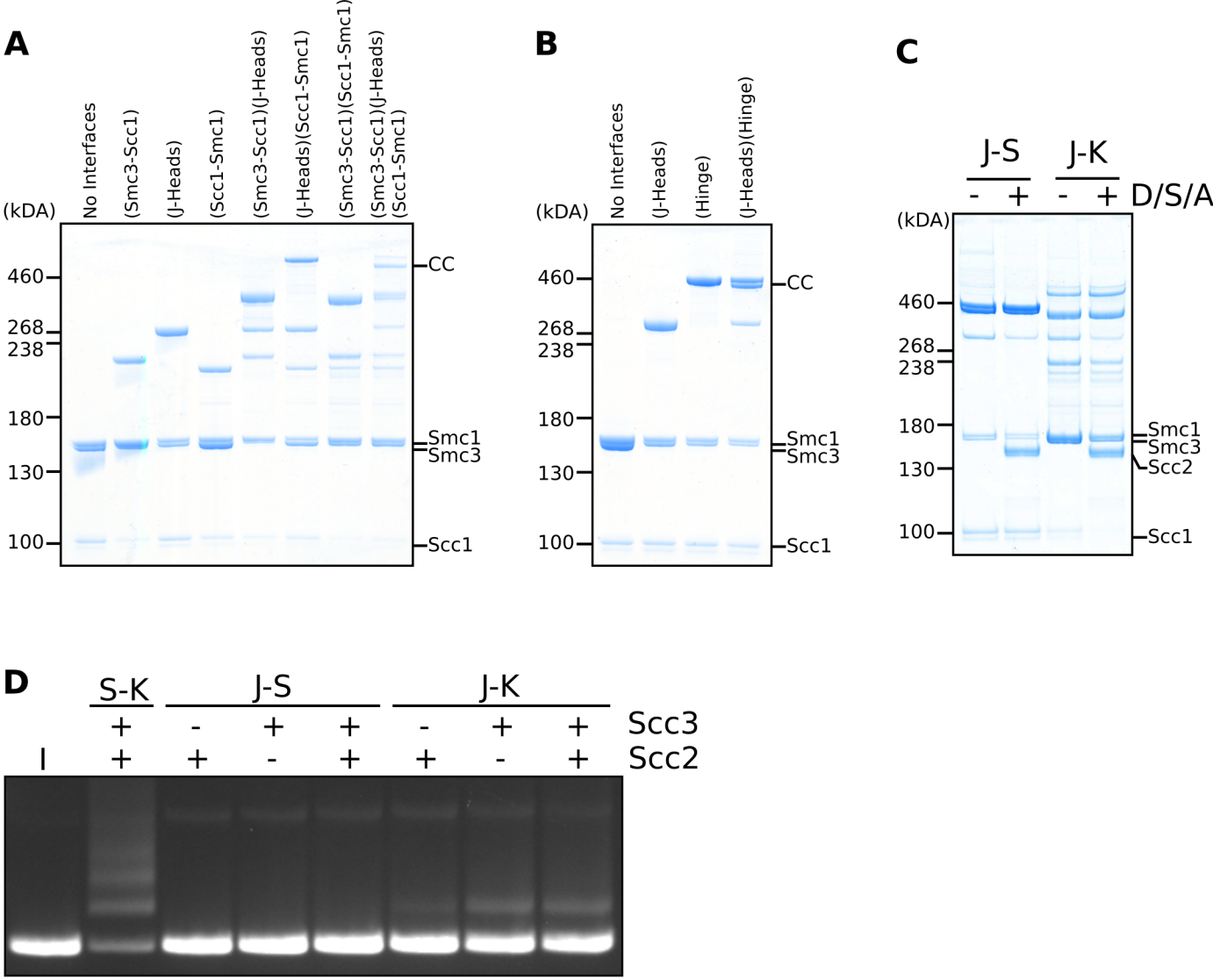
A
No Interfaces
(Smc3-Scc1)
(J-Heads)
(Scc1-Smc1)
(Smc3-Scc1)(J-Heads)
(J-Heads)(Scc1-Smc1)
(Smc3-Scc1)(Scc1-Smc1)
(Smc3-Scc1)(J-Heads)
(Scc1-Smc1)
(kDA)
460
268
238
180
130
100
CC
Smc1
Smc3
Scc1
B
No Interfaces
(J-Heads)
(Hinge)
(J-Heads)(Hinge)
(kDA)
460
268
238
180
130
100
CC
Smc1
Smc3
Scc1
C
J-S
J-K
- + - + D/S/A
(kDA)
460
268
238
180
130
100
Smc1
Smc3
Scc2
Scc1
D
S-K
J-S
J-K
Scc3
Scc2
I
+ - + + - + +
+ + - + + - +

Fig S4

Figure S4. DNA is never entrapped in J-S and only rarely in J-K compartments

(**A**) BMOE crosslinking of J-K compartments, or (**B**) of J-S compartments, with cysteine pairs in the designated interfaces. CC = circular cohesin. (**C**) Crosslinking of J-S or J-K compartments in the presence of DNA, Scc2, and ATP (D/S/A) or absence of all three. (**D**) Entrapment of DNA in either S-K rings, or J-S/J-K compartments in the presence of Scc2, Scc3, or both Scc2 and Scc3. Incubated for 40min. (I = input DNA).

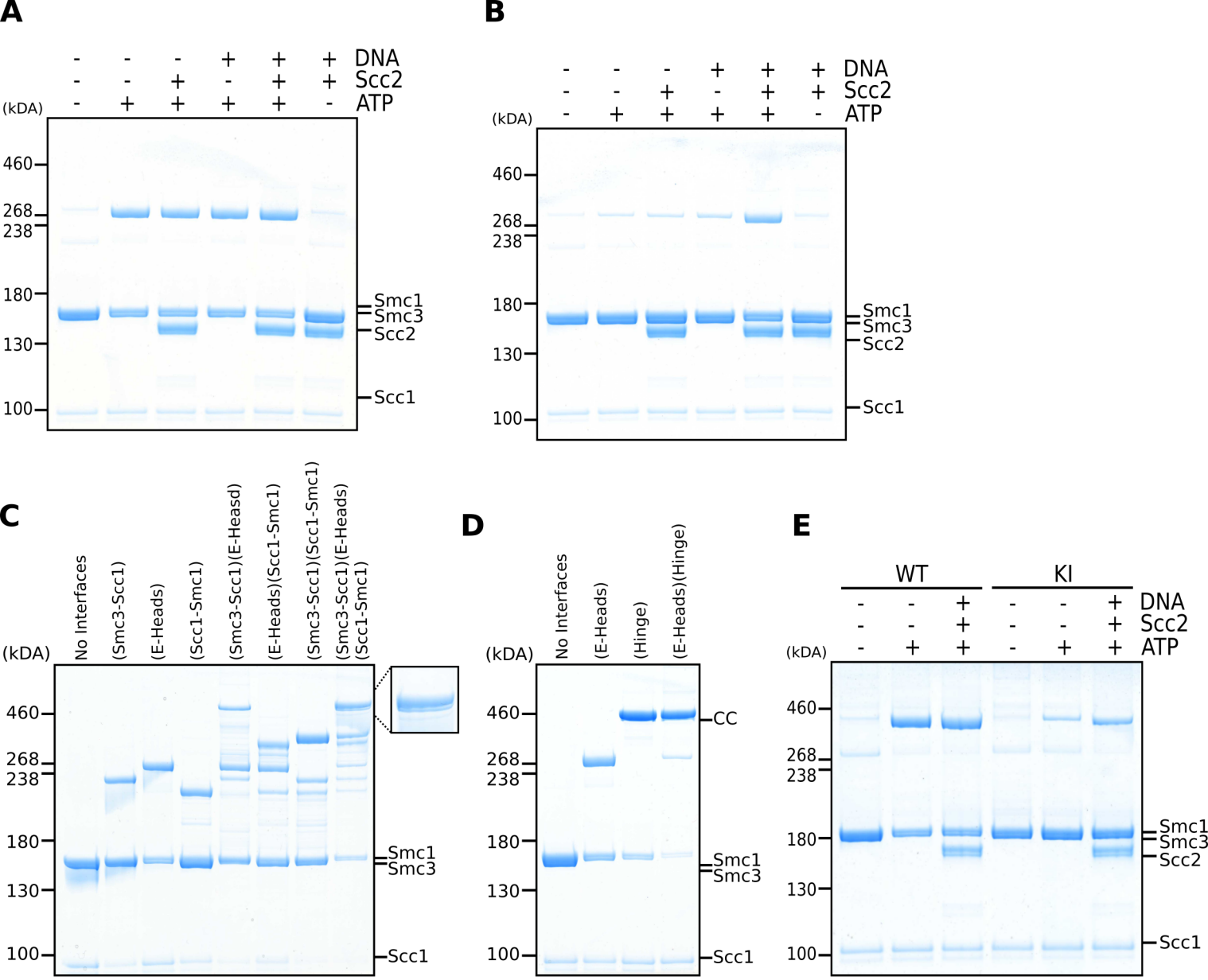
A
DNA
Scc2
ATP
(kDA)
460
268
238
180
130
100
Smc1
Smc3
Scc2
Scc1
B
DNA
Scc2
ATP
(kDA)
460
268
238
180
130
100
Smc1
Smc3
Scc2
Scc1
C
No Interfaces
(Smc3-Scc1)
(E-Heads)
(Scc1-Smc1)
(Smc3-Scc1)(E-Heasd)
(E-Heads)(Scc1-Smc1)
(Smc3-Scc1)(Scc1-Smc1)
(Smc3-Scc1)(E-Heads)(Scc1-Smc1)
(kDA)
460
268
238
180
130
100
Smc1
Smc3
Scc1
D
No Interfaces
(E-Heads)
(Hinge)
(E-Heads)(Hinge)
(kDA)
460
268
238
180
130
100
CC
Smc1
Smc3
Scc1
E
WT
KI
DNA
Scc2
ATP
(kDA)
460
268
238
180
130
100
Smc1
Smc3
Scc2
Scc1

Fig S5

Figure S5. Related to Figure 5

(**A**) BMOE crosslinking of cohesin containing a cysteine pair for E head association, in the presence of ATP, DNA, or Scc2 in various combinations, as well as the presence of 1mM $MgCl_2$, or (**B**) the absence of 1mM $MgCl_2$. (**C**) BMOE crosslinking of E-K compartments, or (**D**) of E-S compartments, with cysteine pairs in the designated interfaces. CC = circular cohesin. (**E**) BMOE crosslinking of cohesin containing a cysteine pair for E head association comparing WT cohesin against Smc3K38I (KI) in the presence of ATP, DNA, or Scc2 in various combinations.

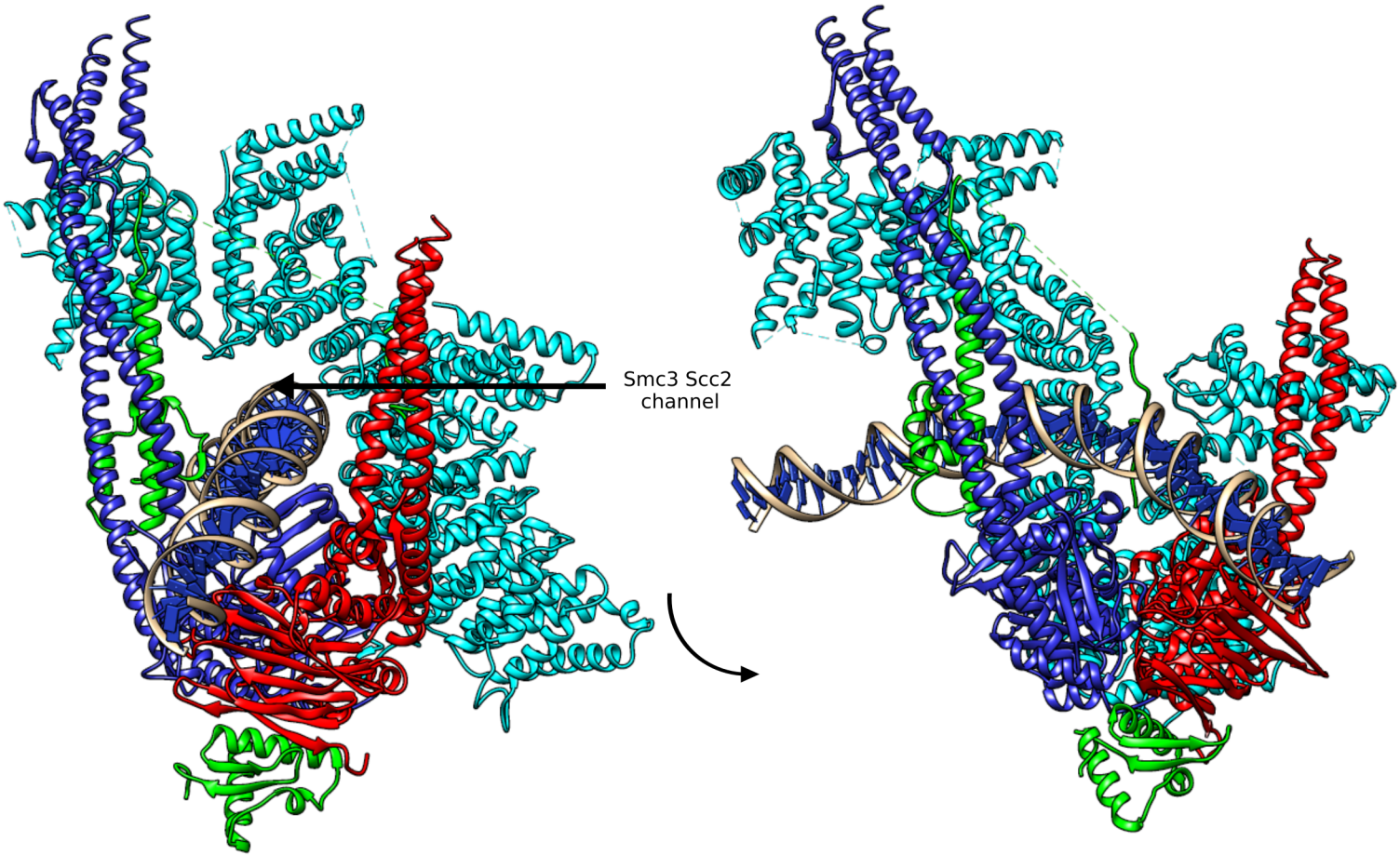

Fig S6

Figure S6. Related to Figures 6 and 7

Cryo-EM structure of NIPBL bound to the Smc1/3 head domains in the E-state (Shi et al., 2020) with DNA bound to positive groove on top of the heads and within a channel made between NIPBL and the Smc3-Scc1 interface. Right-hand panel rotated 45º anticlockwise with respect to the left-hand panel.

KEY RESOURCES TABLE

REAGENTS	SOURCE	IDENTIFIER
Antibodies		
Anti-His (mouse)	Sigma	Cat# SAB1305538-400UL
Anti-mouse HRP	ThermoFisher	**Cat#** 62-6520
Anti-Smc3 (mouse)	Bethyl Laboratories	Cat# A300-060A
Anti-Strep HRP	iba	Cat# 2-1502-001
Bacterial Strains		
DH10Bac	ThermoFisher	Cat# 10361012
PIR1	ThermoFisher	Cat# C101010
TOP10	ThermoFisher	Cat# C404010
Cell Lines		
Sf9	ThermoFisher	Cat# 11496015
Chemicals and Recombinant Proteins		
ATP Lithium Salt	Sigma	Cat# 11140965001
Bismaleimidoethane (BMOE)	ThermoFisher	Cat# 22323
Complete EDTA free protease inhibitor cocktail	Roche	Cat# 4693132001
Cre Recombinase	New England Biolabs	Cat# M0298S
Desthiobiotin	Fisher Scientific	Cat# 12753064
EtBr	ThermoFisher	Cat# 15585011
Fetal Bovine Serum	Sigma	Cat# 12303C
FuGENE HD Transfection reagent	Promega	Cat# E2311
Gibson Assembly Mix	New England Biolabs	Cat# E2611L
HiLoad 16/60 Superdex 200	GE Healthcare	Cat# GE28-9893-35
HiSpeed Plasmid Maxi Kit	Qiagen	Cat# 12663
HiTrap Q HP	GE Healthcare	Cat# GE29-0513-25
Immobilon Western ECL	Millipore	Cat# WBLKS0500
NuPAGE 3-8% Tris-Acetate Protein Gels	ThermoFisher	Cat# EA0378BOX
PMSF	Sigma	Cat# 329-98-6
Quick Coomassie Stain	Generon	Cat# GEN-QC-STAIN-1L
RNase A	Roche	Cat# 10109169001
Sf900 II SFM	ThermoFisher	Cat# 10902104
StrepTrap HP	Fisher Scientific	Cat# 11540654
Supernuclease	SinoBiological	Cat# SSNP01
Superose 6 Increase 10/300 GL	VWR	Cat# 29-0915-96
TCEP	ThermoFisher	Cat# 20490
4xLDS	ThermoFisher	Cat# NP0007
Critical Commercial Assays		
EnzChek phosphate assay kit	Invitrogen	Cat# E6646
Recombinant DNA		
pACEBAC1 *SMC1*-His	This study	N/A
pACEBAC1 *SMC3*	This study	N/A
pACEbac1 *SMC1*-His *SMC3*	This study	N/A
pACEbac1 *SCC2*$^{133-1493}$-2xStrepII	This study	N/A
pACEbac1 *SCC2*-2xStrepII	This study	N/A
pACEbac1 2xStrepII-*SCC3*	This study	N/A
pIDC *SCC1*-2xStrepII	This study	N/A
pIDC S*cc1*$^{269-451}$-2xStrepII	This study	N/A
pIDC S*cc1*$^{150-298}$-2xStrepII	This study	N/A
pIDC His-*SCC4*	This study	N/A
***S. cerevisiae* strains**		

MATa ura::ADH1 promoter-OsTIR1-9myc::URA3 Scc3-PK3-aid::KanMX4 SCC1-HA3::HIS3	This study	KN20783
MATa Scc3-PK3-aid::KanMX4 SCC1-HA3::HIS3	This study	KN20785
MATa/alpha scc3::NatMX4/WT	This study	KN21079
MATa/alpha scc3::NatMX4/WT, leu::Scc3-HA3::LEU	This study	KN21273
MATa Scc1-PK9::KanMX scc2-45::natMX (L545P D575G)	This study	KN22390
MATa Scc1-PK9::KanMX scc2-45::natMX (L545P D575G) lys2::Scc2-HyGMX	This study	KN24185
MATa Scc1-PK9::KanMX scc2-45::natMX (L545P D575G) LYS2::Scc2(S717L,K721E)-HygMX	This study	KN27010
MATa/alpha scc3::NatMX4/WT, leu::Scc3 (K224E, K225E, R226E)-HA3::LEU	This study	KN27539
MATa scc3::NatMX4, Scc1-PK6::TRP1, leu::Scc3-HA3::LEU	This study	KN27542
MAT alpha scc3::NatMX4, Scc1-PK6::TRP1, leu::Scc3 (K224E, K225E, R226E)-HA3::LEU	This study	KN27547
MATa/alpha scc3::NatMX4/WT, leu::Scc3 (K423E, K513E, K520E)-HA3::LEU	This study	KN27696
MATa scc3::NatMX4, Scc1-PK6::TRP1, leu::Scc3 (K423E, K513E, K520E)-HA3::LEU	This study	KN27697
MATa/alpha scc3::NatMX4/WT, leu::Scc3 (K224E, K225E, R226E, K423E, K513E, K520E)-HA3::LEU	This study	KN27763
MATa ura::ADH1promoter-OsTIR1-9myc::URA3, Scc3-PK3-aid::KanMX4, leu::Scc3-HA3::LEU	This study	KN27796
MATa ura::ADH1 promoter-OsTIR1-9myc::URA3, Scc3-PK3-aid::KanMX4 leu::Scc3 (K224E, K225E, R226E, K423E, K513E, K520E)-HA3::LEU	This study	KN27802
MATa ura::ADH1promoter-OsTIR1-9myc::URA3, Scc3-HA3-aid::KanMX4, Scc1-PK6::TRP1, leu::Scc3 (K224E, K225E, R226E, K423E, K513E, K520E)-HA3::LEU	This study	KN27804
MATa ura::ADH1promoter-OsTIR1-9myc::URA3, Scc3-HA3-aid::KanMX4, Scc1-PK6::TRP1, leu::Scc3-HA3::LEU	This study	KN27821
MATa ura::ADH1promoter-OsTIR1-9myc::URA3, Scc3-HA3-aid::KanMX4, leu::Scc3-HA3::LEU, Scc2-PK9::NatMX	This study	KN28075
MATa ura::ADH1 promoter-OsTIR1-9myc::URA3, Scc3-HA3-aid::KanMX4, Scc2-PK9::NatMX, leu::Scc3 (K224E, K225E, R226E, K423E, K513E, K520E)-HA3::LEU	This study	KN28287